PERGAMON

Journal of Structural Geology 25 (2003) 611–631

JOURNAL OF STRUCTURAL GEOLOGY

www.elsevier.com/locate/jstrugeo

Syntectonic granite emplacement at different structural levels: the Closepet granite, South India

Jean-François Moyen[a,*], Anne Nédélec[b], Hervé Martin[a], Mudlappa Jayananda[c]

[a]*Laboratoire Magmas et Volcans, UMR 6524 CNRS, Université Blaise-Pascal, 5 rue Kessler, F-63038 Clermont-Ferrand, France*
[b]*Laboratoire des Mécanismes de Transfert en Géologie, UMR 5563 CNRS, Université Paul-Sabatier, 38 rue des 36-ponts, F-31400 Toulouse, France*
[c]*Department of Geology, Bangalore University, 560056 Bangalore, Karnataka, India*

Received 9 June 2000; received in revised form 22 March 2002; accepted 26 April 2002

Abstract

The Closepet granite, in South India, is a large (400 km long but only 30 km wide), elongate, Late Archaean granitic body. Structural levels from deep crust to upper levels crop out, as evidenced by a shallowing of paleo-depths from north to south all along the Closepet granite. This allows the study of the emplacement of the same granitic body at various crustal levels. Four zones have been identified: a root zone, where magmas are collected in active shear zones; a transfer zone, featuring large-scale magma ascent and crystal–liquid partitioning in the granitic 'mush'; a 'gap', where the mush was filtered, allowing only the liquids to rise; shallow intrusions, filled with this liquid.

The Closepet granite was emplaced syntectonically. Field work and anisotropy of magnetic susceptibility allowed documentation of steep foliations with subhorizontal lineations, both in the root and transfer zones and in the shallow intrusions. Remote sensing evidenced a network of shear zones bounding the Closepet granite. In the porphyritic root and transfer zones, magmas cooled slowly, thus developing strong fabrics during large-scale dextral shearing. Ascent of residual liquids amidst the crystallizing solid framework was not recorded in the fabrics. However, these liquids were channelised through the gap and infilled the homogeneous shallow intrusions, where rapid cooling only permitted the development of feint, although wholly consistent, fabrics.

Keywords: Syn-tectonic granite emplacement; Late-Archaean; South India; Magnetic fabric; Crustal section

1. Introduction

Ascent and emplacement of granitic magmas have been the subject of a lively debate in the last decade (Benn et al., 1998; Clemens, 1998, and references therein). The major controversy dealt with the relative contributions of diapirism (Bateman, 1984) versus dyking (Clemens and Mawer, 1992; Petford, 1996) or a combination of processes between these two end-members and deformation in the host rocks (Paterson and Miller, 1990). Many authors recognised that tectonics often controls magma emplacement, especially in shear zones (e.g. Hutton et al., 1990; D'Lemos et al., 1992; Hutton and Reavy, 1992). The rheological state of the crust (i.e. brittle or ductile) is a primeval parameter, which has been addressed by workers focusing either on the lower crust (Collins and Sawyer, 1996) or on the upper crust (Paterson and Fowler, 1993).

In South India, the huge Late Archaean Closepet batholith provides an unusual opportunity to study the emplacement of granitic magmas at different crustal levels, since it crops out along a natural crustal section spanning 10–13 km in depth, from granulitic lower crust in the South to greenschist-facies upper crust in the North. Due to its elongate shape, the main body of the Closepet batholith has been suggested to be syntectonically emplaced during strike-slip tectonics by Drury et al. (1984) and Jayananda and Mahabaleswar (1991). Nevertheless, northern cogenetic intrusions display more isotropic shapes without obvious magmatic orientations at the outcrop scale (Chadwick et al., 1996). In order to build and discuss a generalised emplacement model, we combine field and microstructural studies with systematic measurements of the anisotropy of magnetic susceptibility (AMS) to unravel the mineral fabrics.

* Corresponding author. Now at: UMR 7566 G2R, Université de Nancy I, BP 239, 54506 Vandoeuvre-lès-Nancy Cedex, France. Tel.: +33-3-83-68-47-49.
E-mail address: jfmoyen@wanadoo.fr (J.F. Moyen).

0191-8141/03/$ - see front matter © 2002 Elsevier Science Ltd. All rights reserved.
PII: S0191-8141(02)00046-9

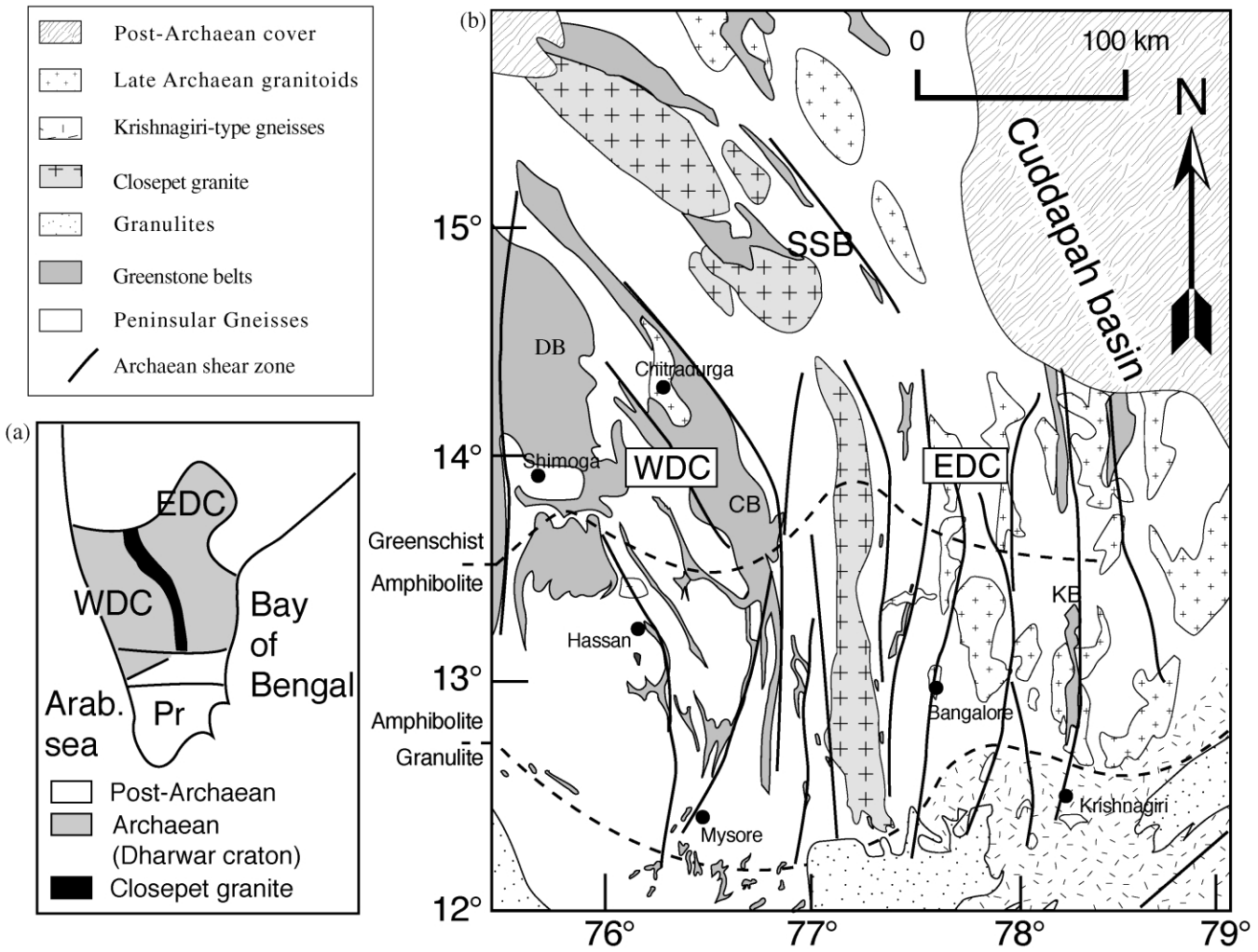

Fig. 1. (a) Sketch map showing the position of the Dharwar craton in South India, with the Closepet granite. WDC, EDC: Western (Eastern) Dharwar Craton; Pr.: Proterozoic domain. (b) Simplified geological map of the Dharwar craton. Abbreviations: SB: Sandur Schist Belt; DB: Dharwar Schist Belt; CB: Chittradurga Schist Belt; KB: Kolar Schist Belt.

2. Geological setting

2.1. The Dharwar craton

The Archaean domain of South India, known as the Dharwar craton, is classically (Windley, 1995) divided into three lithologic units (Fig. 1):

- a gneissic basement of tonalite–trondhjemite–granodiorite (TTG) composition (Barker and Arth, 1976; Martin, 1994), called Peninsular Gneisses and dated between 3.3 and 2.7 Ga (e.g. Taylor et al., 1984; Meen et al., 1992);
- volcanosedimentary greenstone belts unconformably overlying the gneisses, dated between 3.3 and 3.1 Ga for the older ones, and between 3.2 and 2.7 Ga for the younger ones (Peucat et al., 1995);
- Late Archaean, K-rich granitoids, consisting of N–S elongate bodies, among which the Closepet granite is the most spectacular. Several of these granites have been dated in the range 2.5–2.6 Ga (Crawford, 1969; Krogstad et al., 1991; Nutman et al., 1996; Jayananda et al., 2000).

The Dharwar craton is subdivided into Western and Eastern parts (Drury et al., 1984; Bouhallier et al., 1995; Chadwick et al., 2000; Chardon et al., 1998). The Western Dharwar craton is made of 3.0–3.3-Ga-old gneisses and greenstones, with very few 2.5 Ga granites; on the other hand, the Eastern Dharwar Craton is made of younger (2.7–3.0 Ga) rocks with widespread elongate plutons of Late Archaean granites. The Closepet granite represents the boundary between the two parts. Hence, the tectonic setting of the Closepet granite is of key importance to study and constrain the accretion mode of the Late Archaean Dharwar craton.

2.2. Deformation

During the Late Archaean, the Dharwar craton

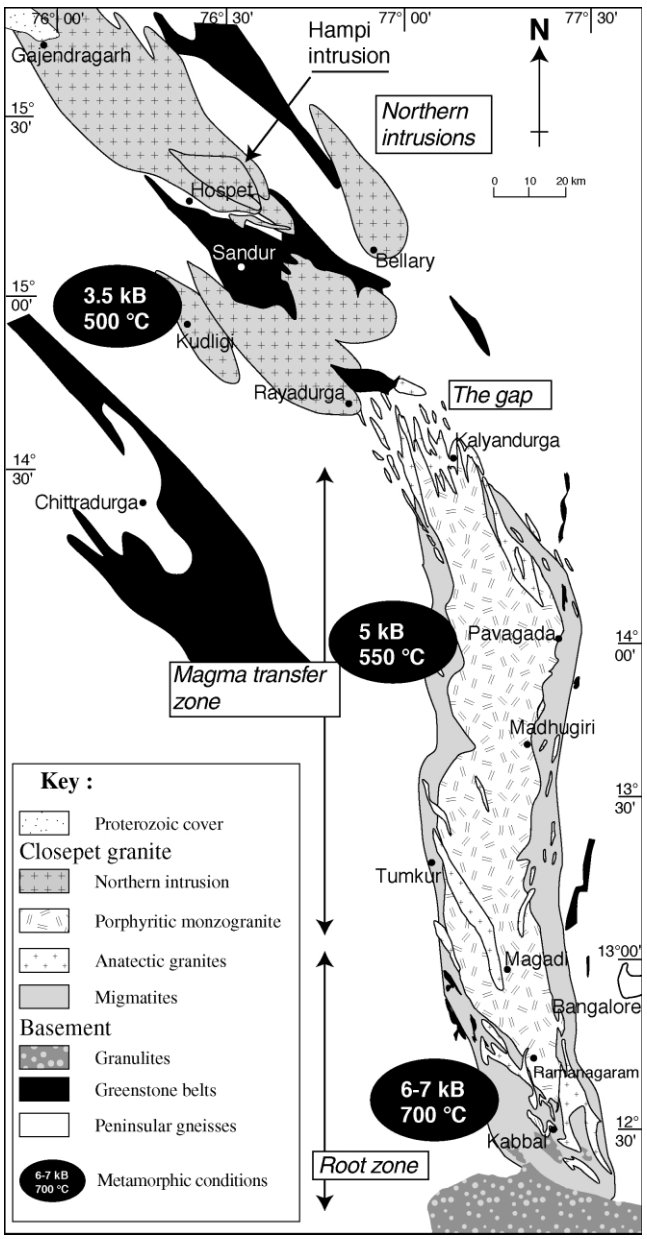

Fig. 2. Geological map of the Closepet batholith. Metamorphic conditions: see references in text.

underwent high temperature metamorphism, reaching granulite-facies conditions in the South. This metamorphism locally induced anatexis of the gneisses (Friend, 1984; Newton, 1990). Ductile deformation, associated with this metamorphism, has been studied by Bouhallier et al. (1995 and Chardon et al. (1996, 1998). They demonstrated that the strain patterns of the Dharwar craton resulted from the action of two kinds of forces:

1. *Volume forces*: the inverse density stratification (dense greenstone belts overlying less dense gneisses) causes the 'sagduction' of the greenstone belts, thus resulting in dome-and-basin structures, where gneissic domes are separated by elongate synclines of greenstones.
2. *Boundary forces*: compressional forces develop an anastomosed network of shear zones that have been mapped using remote sensing by Bouhallier (1995).

It has long been suggested (Drury et al., 1984; Jayananda and Mahabaleswar, 1991; Bouhallier, 1995) that the Closepet granite has been emplaced into one of these active shear zones.

2.3. A crustal cross-section

The Dharwar craton has long been recognised as a natural crustal cross-section (Pichamuthu, 1961; Rollinson et al., 1981). This conclusion is based on a set of geological evidence, the most convincing being the progressive change of metamorphic grade, from granulite-facies rocks in the southern part of the craton, to greenschist-facies rocks in the north. $P-T$ calculations, both in the Peninsular Gneisses (Janardhan et al., 1982; Hansen et al., 1984; Gopalakrishna et al., 1986; Stähle et al., 1987; Sen and Bhattacharya, 1990) and in the metapelites (Srinivasan and Tareen, 1972; Rollinson et al., 1981; Harris and Jayaram, 1982) or mafic rocks (Raase et al., 1986) of the greenstone belts allow quantification of the metamorphic gradient. $P-T$ conditions span from nearly 8 Kb and 800 °C (granulite facies) at 12° latitude, to 3.5 Kb and 500 °C (greenschist facies) at 15°N. Dating of the metamorphism (Buhl et al., 1983; Peucat et al., 1989, 1993; Friend and Nutman, 1991; Bouhallier, 1995; Mahabaleswar et al., 1995) invariably yields metamorphic ages between 2.51 and 2.55 Ga, thus synchronous with the emplacement of the Closepet batholith. Since no fault or other discontinuity separates the northern part of the craton from the southern one, the Dharwar craton does provide an oblique section of a Late Archaean continental crust. This section also crosscuts the whole Closepet batholith. The present horizontal distance between the deepermost and uppermost levels is about 400 km. Using the metamorphic conditions as an estimate of the paleo-depths, it is possible to propose a corresponding vertical distance of about 10–13 km. Consequently, the dip of the present erosion surface relative to the Archaean paleo-depths is about 2°. This small angle is within the error on structural measurements, and as such no corrections are needed when discussing the geometry and structure of the whole batholith.

3. The Closepet batholith

The Closepet batholith is a 400-km-long, and 20–30-km-wide batholith. It consists of two main parts, separated by a so-called 'magmatic gap' (Fig. 2).

In the South, an elongate main mass is chiefly made of a porphyritic monzogranite described by Jayananda et al. (1995) and Moyen (2000). This granite is characterised by 2–5-cm-long phenocrysts of K-feldspar in a matrix consisting of plagioclase (An_{20}), scarce K-feldspar, quartz,

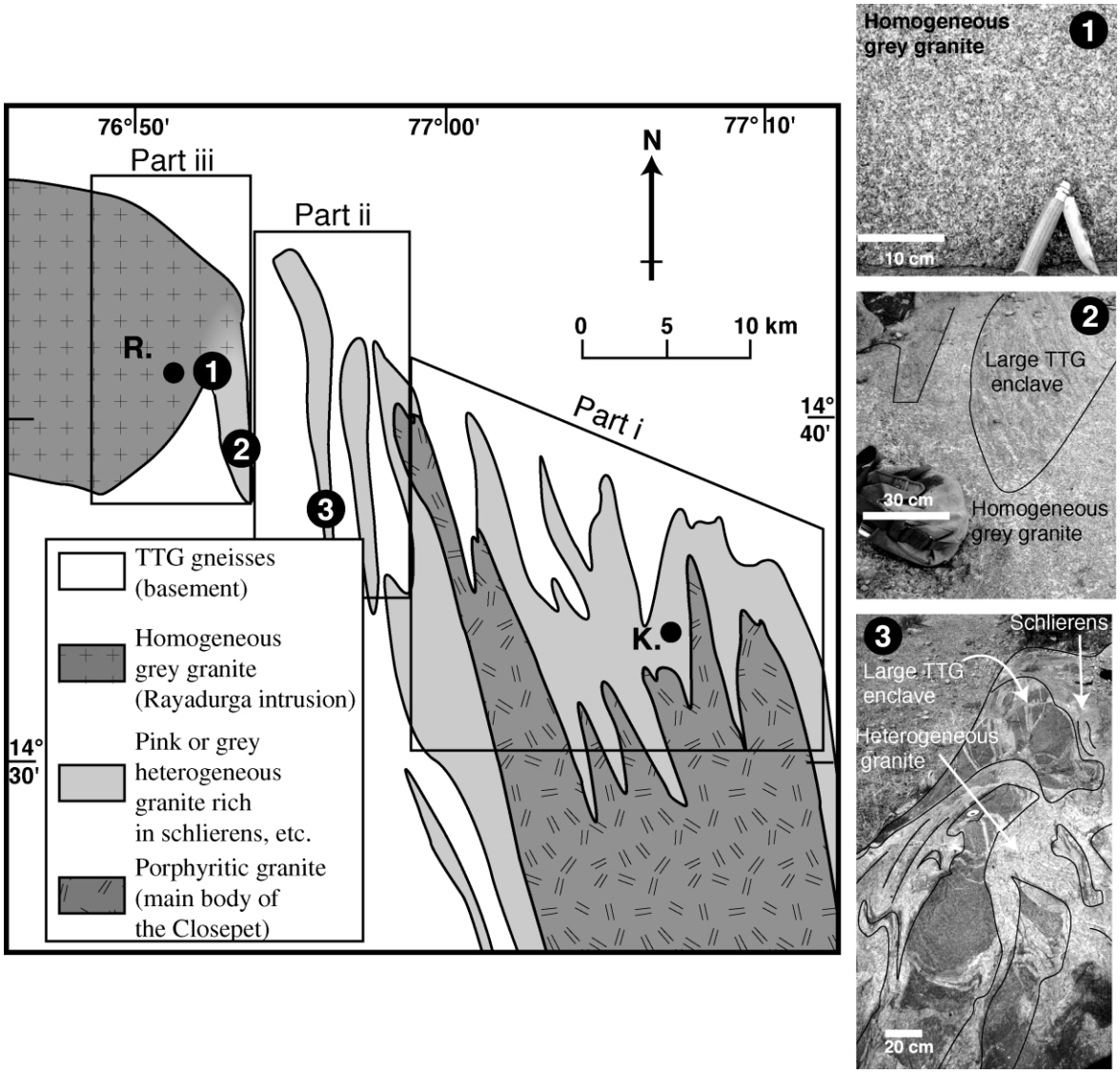

Fig. 3. Geological map of the gap in Rayadurga–Kalyandurga area. Numbers refer to photographs on the right, showing the progressive transition from the 'feeder dykes' to the homogeneous intrusion of Rayadurga. Parts i, ii, iii are described in text.R.: Rayadurga; K.: Kalyandurga.

biotite and amphibole with an average grain size of 1–3 mm. Sphene, apatite, magnetite and ilmenite are the commonly observed accessory minerals. Subordinate rock types are an anatectic granite and large enclaves of clinopyroxene-bearing monzonite. In contrast, the northern intrusions display an elliptic shape and are made of an equigranular, fine- to medium-grained (0.5–3 mm) granite, containing K-feldspar, plagioclase (An_{20}), quartz and biotite. Enclaves and phenocrysts are nearly absent. Between the southern main mass and the northern intrusions, the gap features a network of granitic sheets intruding the Peninsular Gneisses, and connecting both parts of the Closepet batholith.

The southern Closepet granite has been dated by different methods: SHRIMP (Friend and Nutman, 1991); zircon single grain evaporation (Jayananda et al., 1995), Concordia ages on zircons (Buhl et al., 1983) and U–Pb on allanite (Grew and Manton, 1984). All ages fall in the range 2.51–2.53 Ga. In the North, only one age is available: a 2.566 ± 0.03 Ga SHRIMP age obtained by Nutman et al. (1996) on one intrusion immediately north of Sandur Schist Belt. This value almost overlaps the age range obtained in the South. That small age difference, however, is probably not very significant and may be related to slower cooling and freezing of magmas in the deep granulitic crust, than in shallower levels, leading to younger apparent ages in deeper levels.

3.1. The main mass

Based on lithological and structural mapping, the Closepet main mass is further subdivided into a root zone to the south and a transfer zone to the north.

3.1.1. The root zone

This zone extends from the Cauvery river in the south to latitude 13°N (Fig. 2). There, the Closepet granite is mainly made up of coarse-grained porphyritic monzogranite, with subordinate clinopyroxene-bearing monzonite cropping out as large (1–100 m) pillow-shaped bodies. In addition, pink or grey anatectic granites grade into the surrounding gneisses through a thick (up to 10 km) zone of intense migmatization, located at the granite-basement contact (Fig. 2). A striking feature of the root zone is its high lithological heterogeneity: the granite often contains feldspar accumulations, microgranular enclaves, dilacerated basement xenoliths, angular cumulate enclaves and biotite schlierens.

This zone represents the deepest crustal levels, such that it is considered to represent the roots of the granite, where large-scale interactions between the mantle derived magma and the lower crust took place (Jayananda et al., 1995). Based on geochemical modelling, Moyen et al. (2001) deduced the following petrogenesis: (i) a mantle-derived, mafic magma intruded the gneissic crust and induced its partial melting; (ii) the mafic liquid underwent a small (5–10%) amount of fractional crystallization; (iii) both mantle-derived and crustal magmas mixed or mingled together, thus accounting for the diverse chemical and petrological features of the Closepet batholith.

3.1.2. The transfer zone

This zone extends from 13°N to the magmatic gap. As in the root zone, the main petrographic type is the porphyritic monzogranite; it is also associated with anatectic granites at its periphery. Mafic enclaves, xenoliths and feldspar accumulations are restricted to narrow channels, several hundred metres wide, parallel to the general foliation of the Closepet granite. These channels are likely zones of magma ascent, where the crystal-rich inclusions were left behind.

Despite local petrographic heterogeneities, a physical continuity of the porphyritic monzogranite can be observed all over the root and transfer zones. Consequently, the Closepet granite appears as a single magmatic body rather than a track of plutons, as assumed by Chadwick et al. (1996).

3.2. The gap

The geological map of the 'magmatic gap', between Kalyandurg and Rayadurga (Fig. 3) shows the following features from south to north.

To the south (part i), the main mass of the Closepet granite is prolongated by narrow apophyses of porphyritic monzogranite intruded into the Peninsular Gneisses. This part of the gap is also characterised by the abundance of 10–50-m-wide sheets of pink and grey heterogeneous equigranular granites, intrusive into the basement gneisses.

In the central part of the gap (part ii), the porphyritic monzogranite is lacking. There is only a network of heterogeneous sheets of either grey or pink granite within the Peninsular Gneisses.

Close to Rayadurga (part iii), the greyish granite becomes predominant, first as an enclave- and schlieren-rich granite that changes into an homogeneous granite nearly devoid of enclaves and schlierens within a few hundred metres. The enclaves in turn completely disappear a few hundred metres further north in the intrusion zone (Fig. 3).

These observations lead to the conclusion that a link does exist between the main mass and the northern intrusions through the previously alleged 'magmatic gap'. Actually, the gap consists of a network of granitic sheets that connect the heterogeneous southern main mass of the batholith to the homogeneous northern intrusions.

3.3. The Northern intrusions

North of the gap, the granite consists of small (10–50 km in length) ellipsoidal intrusions. The contact with the Peninsular Gneisses is sharp and does not display any migmatization. Each individual intrusion has a granitic composition identical to that of the more differentiated facies from the root and transfer zones. The mafic (clinopyroxene monzonite) and intermediate (porphyritic monzogranite) phases are lacking. The rocks are generally medium-grained, equigranular or weakly porphyritic. The intrusions do not contain any kind of enclave or schlieren, except in a 1-km-wide zone immediately north of the magmatic gap, close to Rayadurga. No fabrics could be observed.

In spite of these differences, these intrusions belong to the Closepet batholith because of the following pieces of evidence: (i) in the field, they are located along strike of the main mass (Fig. 2); (ii) their age is nearly coeval with those obtained in the southern part; (iii) the mineralogical and chemical compositions of these northern granites, as well as the differentiation trends for both major and trace elements, are identical to those of the differentiated facies from the root and transfer zones (Moyen, 2000).

4. Methodology

Besides field work and microstructures study, both anisotropy of magnetic susceptibility (AMS) and remote sensing have been used to characterise the structures of the Closepet granite at different scales.

4.1. Anisotropy of magnetic susceptibility (AMS)

Anisotropy of magnetic susceptibility (AMS) measurements have been done to complement and increase the accuracy of field data. AMS has long been demonstrated (Graham, 1954; Ellwood and Whitney, 1980; Borradaile and Henry, 1997; Bouchez, 2000) as a valuable tool to

Table 1
AMS data for the main mass of the Closepet batholith (south of the gap). *N*: number of specimens; *K*: bulk susceptibility; K_1 and K_3: directions of maximum and minimum susceptibility; *a*: mean deviation from average directions; *P*, *F*, *L*: total, planar and linear anisotropies; *T*: Jelinek parameter

Sample	*N*	GPS localization		*K*	Lineation K_1		Foliation pole K_3		Foliation			$a(K_1)$	$a(K_3)$	*P*	*F*	*L*	*T*
		Lat.	Long.	($\times 10^{-5}$ SI)	Trend	Plunge	Trend	Plunge	Strike	Dip		(°)	(°)				
Root zone																	
Porphyritic monzogranite																	
BH075C	7	12°44′06	77°15′22	9490	192	12	81	49	171	W	41	2	9	1.19	1.04	1.15	−0.60
BH076B	7	12°44′34	77°16′68	4807	174	9	265	5	175	W	85	3	2	1.25	1.18	1.07	0.37
BH084A	4	12°55′45	77°10′12	1376	178	24	276	24	6	E	66	2	4	1.31	1.11	1.20	−0.35
BH168	7	12°57′64	77°12′66	1634	16	33	114	8	24	W	82	2	9	1.3	1.16	1.15	−0.05
Average				*4327*										*1.26*	*1.12*	*1.15*	*−0.16*
Anatectic facies																	
BH071	4	12°45′09	79°25′15	31	347	7	250	39	160	E	51	3	2	1.26	1.17	1.09	0.29
BH072	6	12°29′72	77°22′67	574	166	16	265	28	175	E	62	6	2	1.34	1.28	1.06	0.58
BH074	6	12°46′08	77°20′75	2693	11	34	270	11	2	E	79	7	3	1.68	1.55	1.13	0.55
BH075B	4	12°44′06	77°15′22	5116	177	10	83	23	173	W	67	2	9	1.35	1.09	1.26	−0.52
BH075D	6	12°44′06	77°15′22	10680	24	4	116	2	26	W	88	3	4	1.19	1.10	1.09	−0.01
BH076A	4	12°44′34	77°16′68	5371	353	2	263	7	173	E	83	3	2	1.46	1.34	1.12	0.40
BH078	4	12°50′79	77°70′83	9842	316	53	94	28	4	W	62	3	1	1.39	1.28	1.11	0.37
Average				*4901*										*1.38*	*1.26*	*1.12*	*0.24*
cpx-bearing monzonite																	
BH075A	7	12°44′06	77°15′22	8855	47	59	280	20	10	E	70	23	1	1.28	1.26	1.02	0.83
BH083	4	12°54′31	77°09′43	2814	57	23	303	46	33	E	44	2	2	1.17	1.10	1.07	0.20
BH084B	6	12°55′45	77°10′12	1376	178	11	82	26	172	W	64	1	7	1.22	1.04	1.18	−0.64
Average				*4348*										*1.22*	*1.13*	*1.09*	*0.13*
Average for root zone				**4619**										**1.31**	**1.19**	**1.13**	**0.1**
Transfer zone																	
Porphyritic monzogranite																	
BH081C	4	13°20′21	77°12′69	983	357	0	265	17	175	E	73	2	5	1.22	1.07	1.15	−0.39
BH082	6	13°20′94	77°09′35	788	154	36	351	53	81	S	37	3	2	1.28	1.00	1.12	0.12
BH086	7	13°37′46	77°16′69	3803	170	28	304	52	34	E	38	9	1	1.29	1.24	1.05	0.61
BH089	6	13°40′04	77°11′12	1557	12	6	279	34	9	E	56	3	3	1.37	1.23	1.14	0.16
BH090B	5	13°40′53	77°09′68	1091	2	30	250	30	160	E	60	2	2	1.49	1.35	1.14	0.36
BH094	4	13°51′10	77°06′56	920	171	2	263	50	173	E	40	2	3	1.23	1.10	1.13	−0.19
BH095	7	13°52′62	77°10′19	1227	173	6	270	34	0	E	56	3	1	1.49	1.36	1.12	0.44
BH098	3	14°06′65	77°18′99	1618	161	20	275	48	5	E	42	3	2	1.54	1.34	1.20	0.15
BH099	6	14°07′13	77°18′60	2073	194	14	287	13	17	E	77	3	2	1.56	1.39	1.17	0.31
BH100	5	14°06′64	77°17′26	3357	175	0	265	44	175	E	46	2	2	1.45	1.25	1.20	−0.01
BH104	2	14°10′43	77°04′68	880	1	8	262	39	172	E	51	2	3	1.25	1.12	1.13	−0.10
BH108	8	14°30′51	77°11′63	4422	178	8	275	26	5	E	64	4	2	1.33	1.24	1.09	0.40
BH113	4	14°29′58	77°02′59	2751	359	19	108	43	18	W	47	4	2	1.57	1.45	1.12	0.48
BH265	6	14°03′15	77°06′58	1224	184	3	275	36	5	E	54	2	2	1.40	1.21	1.19	−0.04

(*continued on next page*)

Table 1 (*continued*)

Sample	*N*	GPS localization		*K*	Lineation K_1		Foliation pole K_3		Foliation			$a(K_1)$	$a(K_3)$	*P*	*F*	*L*	*T*
		Lat.	Long.	($\times 10^{-5}$ SI)	Trend	Plunge	Trend	Plunge	Strike	Dip		(°)	(°)				
BH268	5	13°56′85	77°15′05	4716	140	13	256	61	166	E	29	2	2	1.61	1.36	1.25	0.06
BH269	8	13°57′29	77°12′54	2574	10	3	280	9	10	E	81	1	2	1.48	1.24	1.24	−0.09
BH271	4	14°00′84	77°07′98	921	0	2	268	37	178	E	53	3	3	1.23	1.14	1.09	0.14
BH277	5	14°10′56	77°15′83	1466	159	16	261	37	171	E	53	2	2	1.28	1.15	1.13	0.03
BH280	5	14°16′59	77°11′02	4948	87	18	235	67	145	E	23	3	2	1.53	1.38	1.15	0.37
Average				*2175*										*1.40*	*1.24*	*1.15*	*0.15*
Anatectic facies																	
BH080	4	13°10′94	77°17′16	4689	179	19	279	21	9	W	69	1	3	1.65	1.29	1.36	−0.20
BH081A	4	13°20′21	77°12′69	422	1	0	271	27	1	E	63	4	2	1.33	1.21	1.12	0.58
BH090A	7	13°40′53	77°09′68	1352	350	30	242	30	152	E	60	2	4	1.44	1.18	1.26	−0.26
BH111	4	14°31′57	77°05′78	8	292	27	34	36	124	S	54	4	3	1.09	1.06	1.03	0.24
BH115	4	14°27′65	76°59′57	2238	163	15	278	57	8	E	33	2	3	1.38	1.26	1.22	−0.24
BH290	4	14°41′44	76°51′77	442	158	49	258	10	168	E	80	2	2	1.42	1.24	1.18	0.09
Average				*1525*										*1.39*	*1.21*	*1.2*	*0.04*
Average for transfer zone				**2019**										**1.40**	**1.23**	**1.16**	**0.12**

Table 2
AMS data for the northern intrusions (North of the gap); see Table 1 for explanation of parameters

Sample	N	GPS localization		K	Lineation K_1		Foliation pole K_3		Foliation			$a(K_1)$	$a(K_3)$	P	F	L	T
		Lat.	Long.	($\times 10^{-5}$ SI)	Trend	Plunge	Trend	Plunge	Strike	Dip		(°)	(°)				
Hampi granite																	
BH307	6	15°19′11	76°28′81	504	132	19	51	29	121	S	61	5	2	1.14	1.06	1.04	0.35
BH308	4	15°19′42	76°29′61	283	163	58	46	16	136	W	74	4	2	1.18	1.12	1.06	0.32
BH309	4	15°19′47	76°30′05	152	281	70	40	8	130	S	82	12	2	1.22	1.18	1.04	0.62
BH310	4	15°19′71	76°30′62	349	146	13	53	8	143	W	82	4	1	1.28	1.22	1.06	0.53
BH311	3	15°20′71	76°31′41	300	148	11	241	13	151	E	77	4	6	1.16	1.07	1.09	−0.13
BH312	4	15°21′89	76°32′20	332	157	12	253	3	163	E	87	4	2	1.27	1.20	1.07	0.40
BH313	6	15°22′15	76°33′68	153	331	26	241	0	151	E	90	3	2	1.32	1.24	1.08	0.47
BH317	5	15°21′21	76°24′90	530	321	2	50	8	140	W	82	2	3	1.38	1.20	1.18	−0.02
BH318	4	15°20′92	76°27′25	740	155	5	246	5	156	E	85	3	3	1.29	1.14	1.15	−0.11
BH319	5	15°21′42	76°28′54	690	140	32	236	9	146	E	81	3	2	1.25	1.17	1.08	0.28
BH320	4	15°21′71	76°29′58	756	140	12	233	14	143	E	76	2	2	1.27	1.16	1.11	0.10
BH321	4	15°22′99	76°30′79	1462	358	5	265	26	175	E	64	3	1	1.23	1.17	1.06	0.42
BH322	4	15°24′15	76°32′03	942	117	0	208	0	118	N	90	3	1	1.35	1.28	1.07	0.40
BH324	5	15°25′08	76°20′18	860	338	1	68	38	158	W	52	12	2	1.13	1.09	1.04	0.45
Average				*537*										*1.25*	*1.16*	*1.08*	*0.29*
Surrounding pink granites																	
BH129	4	15°32′94	76°23′06	1731	36	75	262	12	172	E	78	2	1	1.44	1.29	1.15	0.25
BH306	4	15°17′95	76°26′75	951	157	33	288	46	18	E	44	1	2	1.29	1.14	1.15	−0.13
BH314	5	15°21′00	76°20′54	2321	149	11	243	20	153	E	70	2	2	1.25	1.14	1.11	0.07
BH315	6	15°20′84	76°21′47	672	166	15	64	20	154	W	70	2	5	1.13	1.04	1.09	−0.40
BH316	5	15°20′87	76°23′18	852	151	7	241	8	151	E	82	2	6	1.19	1.06	1.13	−0.43
BH323	4	15°24′68	76°19′60	580	159	12	250	6	160	E	84	3	3	1.16	1.09	1.07	0.04
Average				*1185*										*1.24*	*1.13*	*1.12*	*−0.10*
Average for northern intrusions				**731**										**1.25**	**1.15**	**1.09**	**0.17**

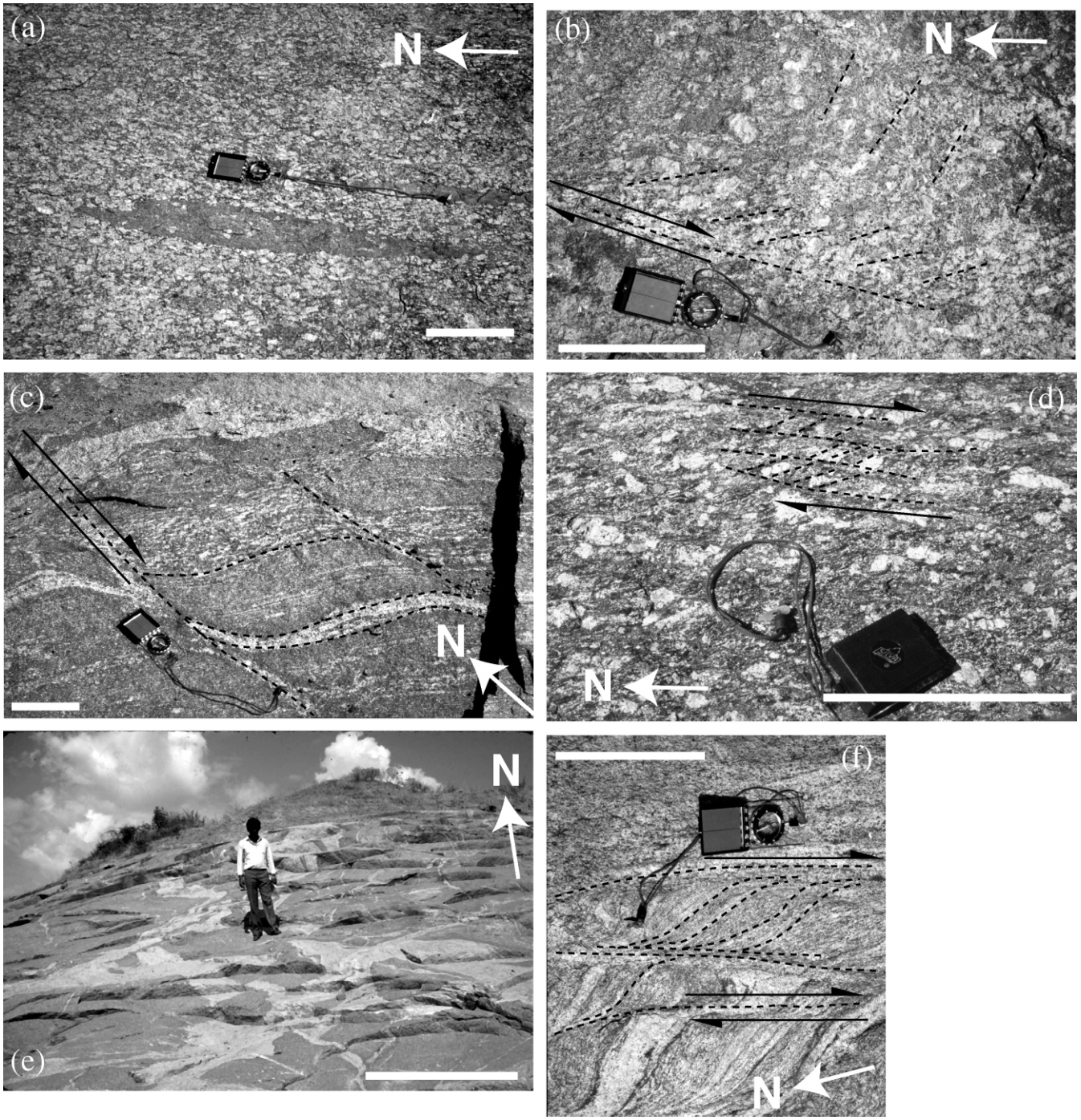

Fig. 4. Outcrop picture exemplifying the various deformation-related features within the root zone. Bar scale is 20 cm on all pictures except (e) (2 m). All pictures on horizontal planes, except (e) (oblique surface). (a) A well-defined foliation is underlined by preferred orientation of K-feldspar megacrysts, enclaves flattening and schlierens (Site BH 13, 7 km E of Ramanagaram). (b) K-feldspar megacrysts are reoriented in N20 in a syn-magmatic shear zone cutting across the N160 foliation (BH 76, 10 km N of Ramanagaram). (c) Magmas mixing between different facies show a N120 foliation which is cut by a late, N10 shear zone invaded by aplito-pegmatitic pink granite (BH 75, 5 km N of Ramanagaram). (d) C/S fabric in the porphyritic granite (BH 100, Pavagada quarry). (e) Magma mingling in the root zone causes disorganisation of the foliation (BH 75, 5 km N of Ramanagaram; same outcrop as (c)). (f) Foliation and shear zones in migmatites around the Closepet granite (BH 74, Eastern margin of Closepet granite, Tumkur–Bangalore road).

characterise the fabric in granitic rocks, especially when no mesoscopic fabric is visible in the field. Sixty-five oriented rock samples (each about 1 dm^3 in volume) were collected from different places in the Closepet granite. In some cases, several samples were picked up from the same site to account for the lithological diversity. Twenty samples came from three parallel cross-sections in a single, well-identified intrusion in the northern part of the Closepet Batholith, the Hampi intrusion (Fig. 2). The remaining samples were collected in the main mass of the Closepet granite. In the

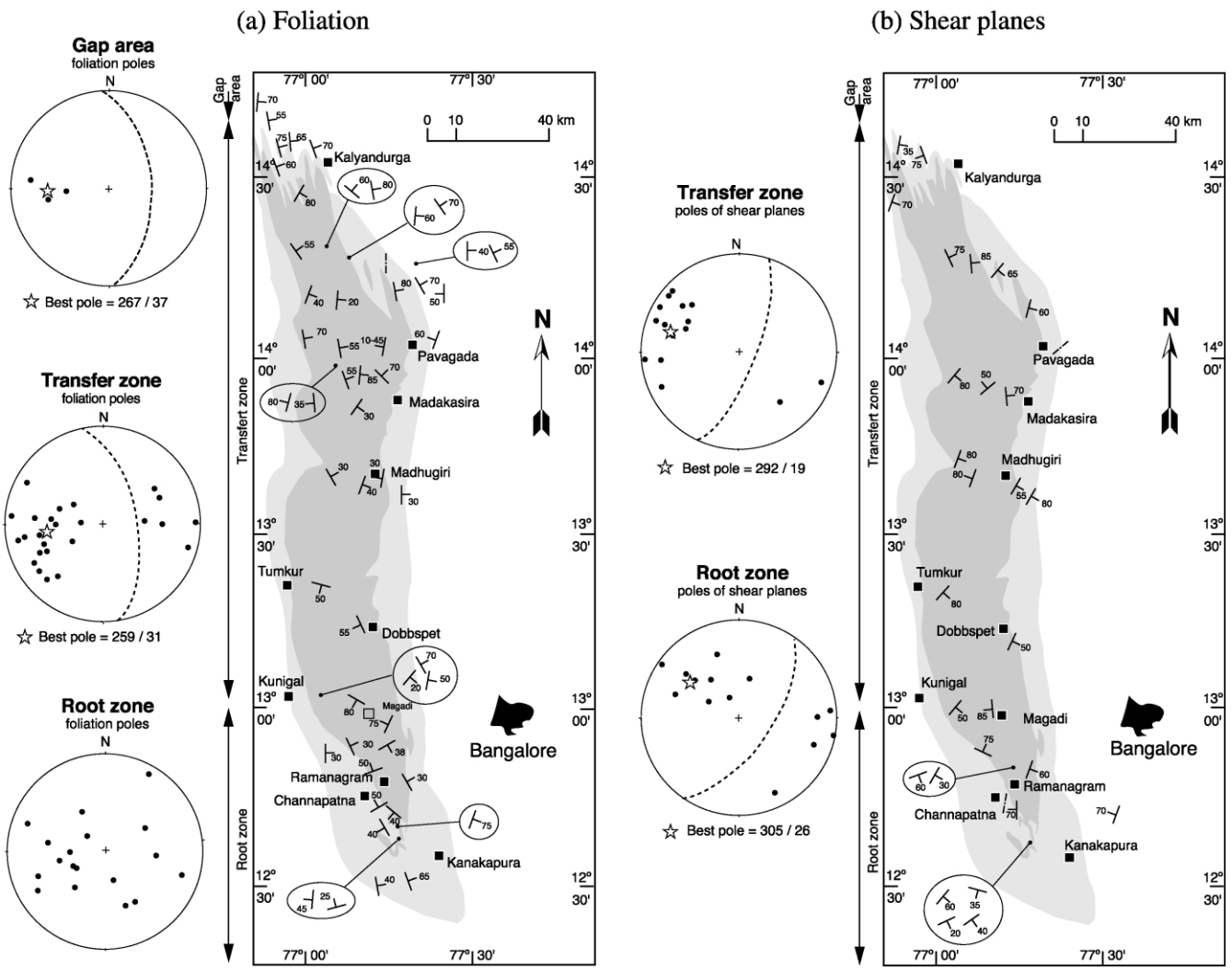

Fig. 5. (a) Map of the foliation plane and S planes in C/S structures in the main mass of the Closepet granite. (b) Map of the shear planes and C planes in C/S structures in the main mass. All stereograms are Schmidt equal area projection, lower hemisphere. Pole of planes: dots; pole of the best great circle: star.

laboratory, each sample was processed using the method described by Bouchez (1997). Three to eight cylindrical specimens (2.5 cm in diameter and 2.2 cm in length) were extracted from each sample. Each specimen was oriented with respect to the geographic frame and measured for AMS determination, using a Kappabridge KLY-2 susceptometer (AGICO, Brno), working at low alternative inducing field (4.10^{-4} T, 920 Hz), with a sensitivity better than 5.10^{-8} SI units. Results are presented in terms of both magnitude and orientation of the main axes (K_1, K_2, K_3) of the AMS ellipsoid in Tables 1 and 2.

Magnetic susceptibility magnitudes are generally very high, ranging from 8×10^{-5} to 10680×10^{-5} SI units (mean value around 3000×10^{-5}) in the main mass, and from 150×10^{-5} to 2320×10^{-5} SI units in the northern intrusions (mean value: 730×10^{-5}). The anatectic granites display a high variability: low susceptibility values are associated with leucosome-rich rocks and high susceptibility with restite-rich rocks. Most samples yield values much higher than 50×10^{-5} SI and, therefore, can be interpreted in terms of dominant ferromagnetic behaviour (Rochette, 1987; Rochette et al., 1992), due to the presence of abundant magnetite, a common situation in I-type granitoids (Ishihara, 1977). Moreover, apart from the anatectic facies, a rough correlation exists between petrographic types and bulk susceptibilities, reflecting the rock magnetite contents as observed by Déléris et al. (1996). For instance, high susceptibility values are observed in the monzonite from the main mass, whereas low values are typical of the leucocratic Hampi granite belonging to the northern intrusions. The magnetic fabric of such magnetite-bearing granites strongly depends on the grain shape fabric of primary magnetite grains and is generally similar to the overall petrofabric of the rock (Grégoire et al., 1998; Launeau and Cruden, 1998). Therefore, K_1 is the magnetic (and mineral) lineation, and K_3 is the pole of the magnetic (and mineral) foliation plane. The mean angular deviations $a(K_1)$ or $a(K_3)$ between each individual specimen measurements and the tensorial averages K_1 or K_3 for the corresponding sample are less than 5° in 92% of samples.

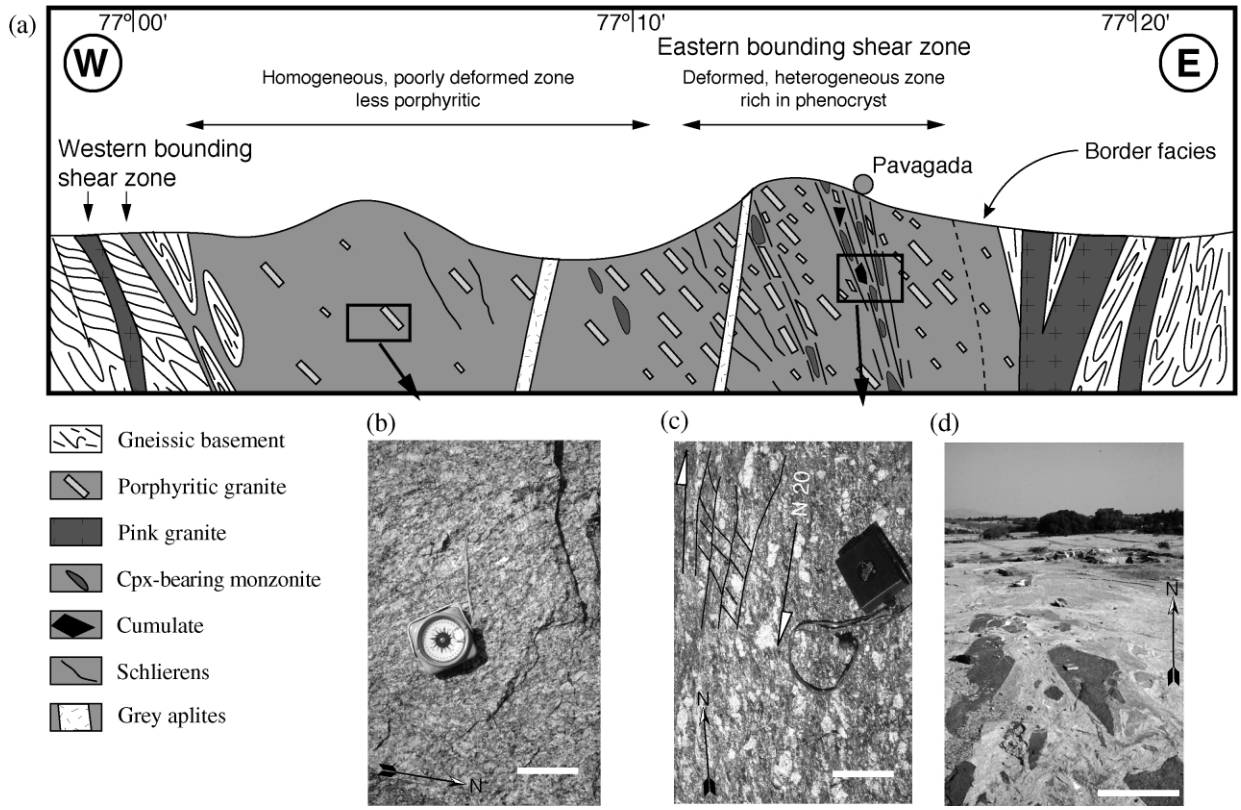

Fig. 6. (a) Cross-section in the Closepet granite at the latitude of Pavagada (14°N). It is mainly made of a weakly porphyritic granite with occasional C/S fabric or shear zone, but in one area located close to the Eastern boundary of the Closepet, a high-strain zone is rich in enclaves of all kinds, originating in the deeper crustal levels. (b) Slightly porphyritic, homogeneous granite (BH 271, 20 km W of Pavagada). (c) C/S fabric (BH 100, Pavagada quarry). (d) Enclave-rich corridor (BH 100, Pavagada quarry, looking N). Scale bar is 10 cm in (b) and (c), and 1 m in (d). (b) and (c) are pictures of an horizontal plane.

These results point to the constancy of the magnetic fabric at the sample scale, hence to the validity of the method. Tables 1 and 2 also report the usual anisotropy parameters, which are the total ($P = K_1/K_3$), planar ($F = K_2/K_3$) and linear ($L = K_1/K_2$) anisotropies, and the T parameter (Jelinek, 1981) describing the shape of the AMS ellipsoid (prolate for $-1 < T < 0$, oblate for $0 < T < 1$).

4.2. Remote sensing

Remote sensing has long been used to characterise strain patterns in the upper crust; more recently, it was demonstrated that it is also a powerful tool for large-scale ductile structure mapping. Martelat et al. (1995) discussed the possible origin of the SPOT signal in relation to field structures, in a high-grade terrane from a dry tropical area with scarce vegetation in southern Madagascar, which is very similar to the Closepet area. They concluded that the signal is mainly due to lithologic contrasts parallel to the foliation planes as a result of tectonic transposition. Therefore, the SPOT trails may be interpreted in terms of foliation or ductile shear zone strikes.

Two multispectral images acquired by the satellite SPOT over the southern part of the Closepet main mass were used: scene 215-324 from 14-05-89 and scene 215-325 from 14-05-89. For each image, the three monochromatic channels were treated by dynamic stretching. A coloured composition was then build and corrected for geometric deformations due to the orbital path of the satellite. No further processing was performed and images were then redrawn for tracing of the main lineaments and interpretation after assembly. Geological boundaries were also drawn from (i) previously published maps (Jayananda et al., 1995; Moyen et al., 1997); (ii) our field work; and (iii) colour or textural differences observed on the images. Further North, we used 'quicklooks' (low-resolution images) provided by SPOT image.

5. Structural data

5.1. Main mass

5.1.1. Field data

Foliations and shear planes were recognised in the field and are presented in Fig. 4. Foliations are characterised by a planar disposition of K-feldspar phenocrysts in the porphyritic granite (Fig. 4a), more or less elongate microgranular mafic enclaves, schlierens of restitic biotite (in the anatectic granite only). In the transfer zone, foliations strike broadly north–south with a medium to steep dip towards the east. The average foliation plane strikes N159E and dips 59°

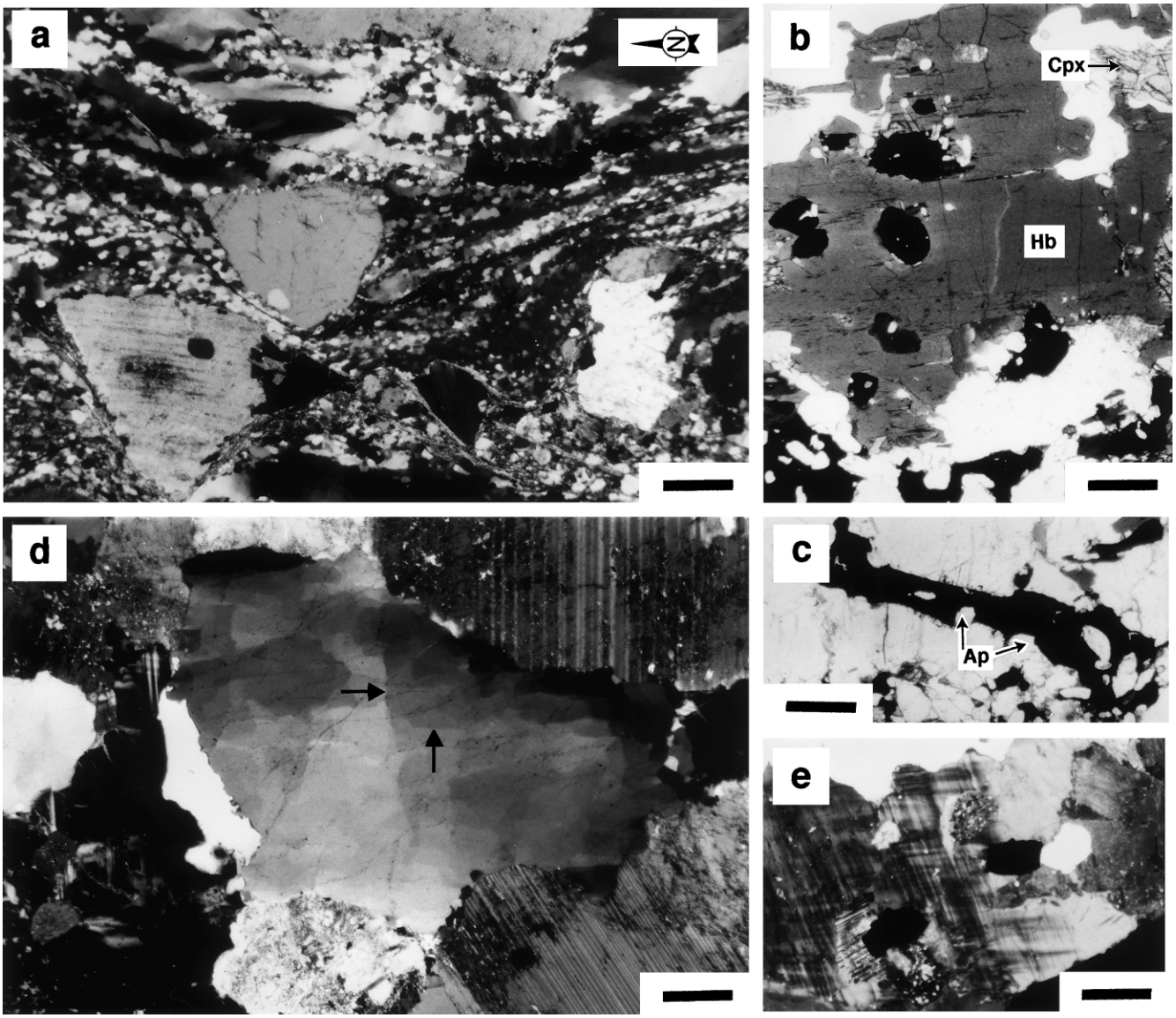

Fig. 7. Microphotographs with crossed polars ((a), (d), (e)) or plane polarized light ((b), (c)); scale bar: 1 mm. (a) Mylonitic texture in porphyritic granite BH 269 from transfer zone (*XZ* section). (b) Numerous grains of oxide minerals (magnetite) in monzonite BH 78; Cpx: clinopyroxene; Hb: hornblende. (c) Elongate cluster of accessory minerals (oxides and apatite: Ap) in monzonite BH 75. (d) Chessboard pattern of quartz subgrain boundaries (arrows) in quartz from Hampi granite BH 307. (e) Euhedral oxides in granite BH 315 (close to Hampi intrusion).

towards the east (159 E 59) (Fig. 5). This direction corresponds to the longest axis of the Closepet granite. In some places, the porphyritic granite appears to be orthogneissified, with sigmoidal phenocrysts. As evidenced by microstructures (see Section 5.1.2 below), the fabric developed from magmatic to solid-state conditions.

Shear zones were also recognised (Fig. 4b and c); they strike NE to NNE and dip steeply to the east (Fig. 5). Depending on formation temperature, they show diffuse contact with their host rocks (Fig. 4b and c) and may be invaded by late pink granites, or they are occasionally filled by epidote indicating that shearing remained active down to greenschist facies conditions. In some places, C/S structures (Fig. 4d) developed before full crystallization or at the solid state, as described elsewhere by Berthé et al. (1979) and Gapais (1989). The shear zones are irregularly spaced, about 1–10 m apart from each other. The apparent horizontal displacement ranges between 10 cm and 1 m (Fig. 4c). Most of them are dextral. In the root and transfer zones, the patterns are similar. However, foliation and shear planes are more scattered in the root zone, due to the moulding of metric-scale mafic blobs in numerous mingling areas (Fig. 4e). Analogous structures can be observed in all granitic facies and also in the migmatitic cortex of the Closepet granite (Fig. 4f). In the transfer zone, the high-strain shear zones are 0.1–1 km in width and enclave-rich (Fig. 6), suggesting that residual liquid has been lost by upward transfer. Outside these deformed zones, the Closepet granite consists of a porphyritic facies with a magmatic foliation.

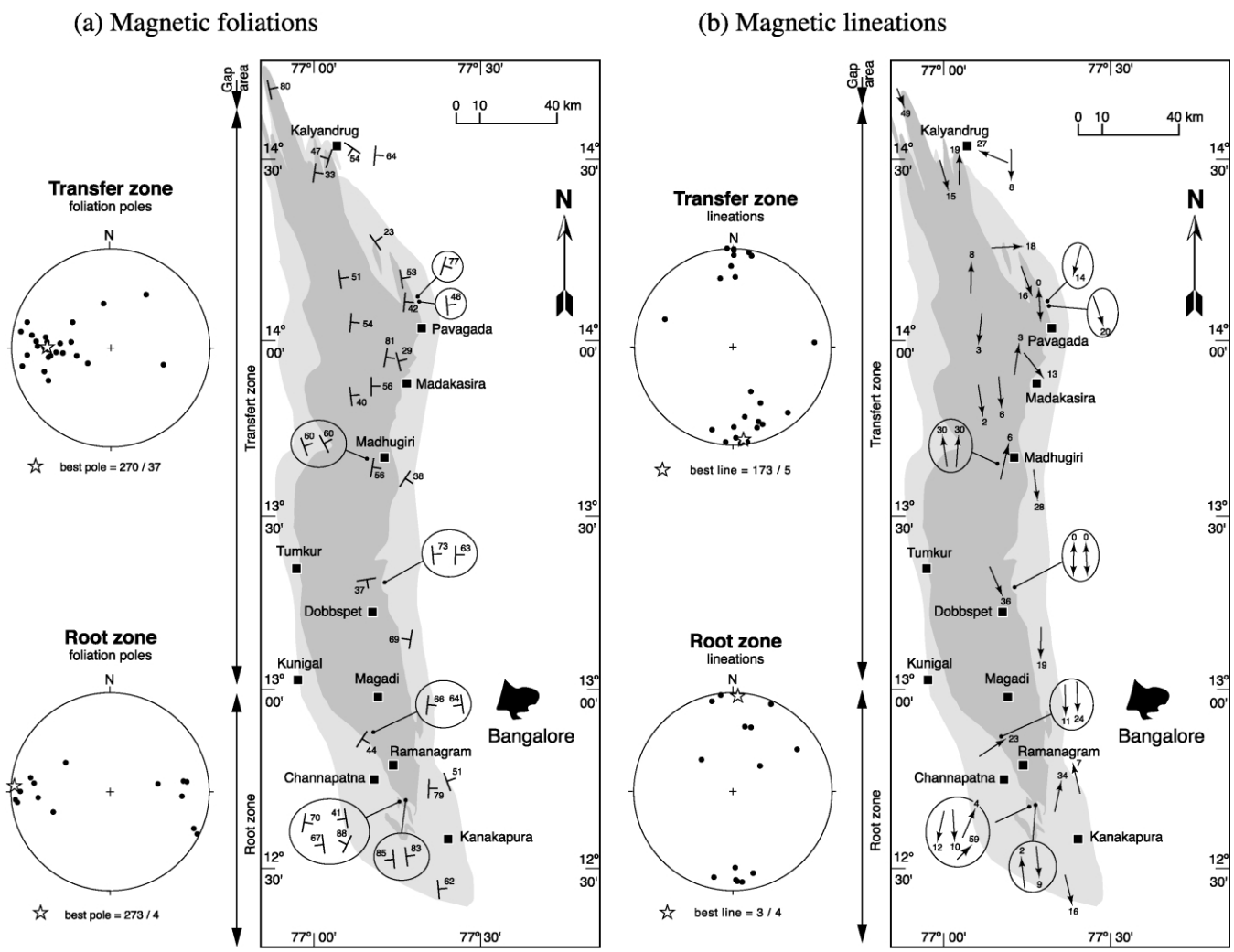

Fig. 8. AMS foliations (a) and lineations (b) in the main mass of the Closepet granite.

5.1.2. Microstructures

Microstructures span the whole range between typically magmatic to mylonitic (Fig. 7a). In most cases, the rocks with magmatic microstructures display incipient solid-state deformation in near-solidus conditions, as evidenced by the occurrence of both prismatic and basal subgrains responsible for typical chessboard patterns in quartz (Bouchez et al., 1985; Kruhl, 1996). Protomylonitic to mylonitic rocks were plastically deformed in the solid state at high-temperature conditions, as evidenced by the lack of retrogressed mineral assemblages. Consistent orientations in both magmatic and mylonitic rocks point to the same deformation regime, all over the supra-to-sub solidus transition.

Opaque minerals (including magnetite) are either subhedral (Fig. 7b) or interstitial, and often belong to elongate clusters of ferromagnesian and accessory minerals (Fig. 7c). Their shape is generally elongate, with shape ratios up to three, and their long axis is roughly parallel to the magmatic or mylonitic foliation planes. These observations testify that the magnetic fabric mimics either the magmatic fabric or the mylonitic fabric, depending on the intensity of the deformation suffered by the rocks.

5.1.3. AMS data

Magnetic foliation and lineation maps are presented in Fig. 8, together with projection diagrams of magnetic foliation poles and magnetic lineations for the root and transfer zones. Most samples display a strong anisotropy (P up to 1.65, mean values ranging between 1.30 and 1.40: see Table 1). These high anisotropy values characterise ferromagnetic granitoids with a pronounced magmatic foliation or even orthogneissified rocks (Saint Blanquat and Tikoff, 1997; Nédélec et al., 2000). The highest anisotropies (average $P = 1.40$) characterise the high strain areas in the transfer zone. In the root zone, the anisotropies are slightly lower (average $P = 1.31$). Over the whole area, the shape of the AMS ellipsoid is variable, but rather oblate.

Magnetic foliations strike north–south; they are subvertical on average in the root zone, and they dip steeply to the east in the transfer zone (Fig. 8a). There is a general agreement with the planar structures recognised in the field.

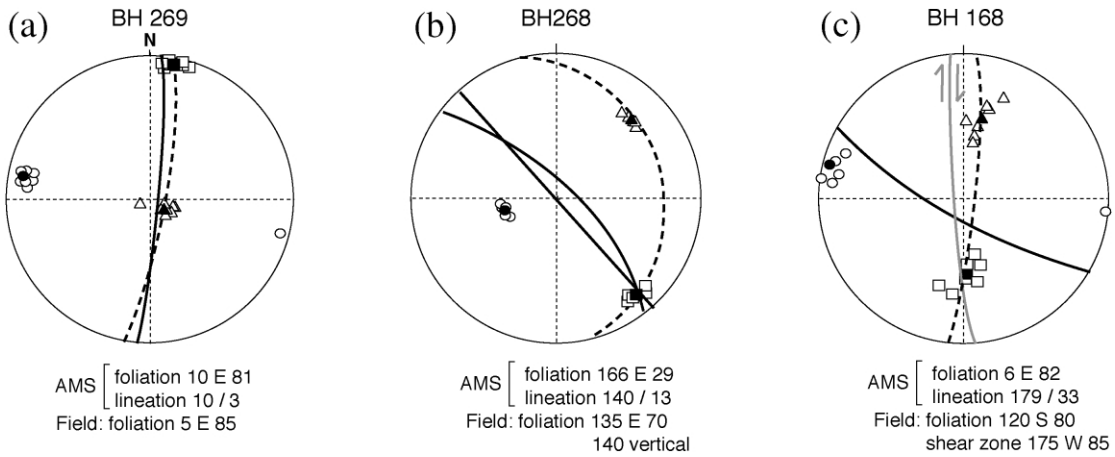

Fig. 9. Comparison between AMS and field data. In all stereoplots, AMS foliation is represented by dashed line; K_1, K_2 and K_3 are, respectively, squares, triangles and circle; hollow symbols are individual measurements, while filled symbols are averages for one sample. Black line: foliation as measured in the field; Thick grey line with motion sense: shear zone as measured in the field. Site localisation: see Table 1.

Nevertheless, the magnetic foliations display much less scatter than field measurements in the root zone (Fig. 5). In the transfer zone, where foliations are easier to determine in the field, most samples show a very good agreement between field and AMS data and the small differences fall within the field measurement accuracy (Fig. 9a). Rare discrepancies are easily explained. For instance, a mineral lineation (corresponding to the magnetic lineation) was likely mistaken for the foliation trace on a subhorizontal bedrock (Fig. 9b); in places where C/S structures were observed, the magnetic foliation may coincide with the shear plane measured in the field (Fig. 9c). In many cases, AMS measurements are considered to provide a better determination of the fabric orientation than field measurements, because they integrate the whole volume of the samples (Bouchez, 1997, 2000).

Still more important, AMS measurements help in determining lineations that were impossible to measure in the field. Lineations are north–south and horizontal on average all along the main mass of the Closepet granite (Fig. 8b).

5.1.4. Remote sensing

Remote sensing enabled distinction of an anastomosing network of high-strain zones characterised by abundant, sinuous, sub-parallel trails, from low-strain zones that display only few lineaments (Fig.10). The direction of metric or decametric shear zones observed in the field are consistent with the high-strain zones mapped via remote sensing. The main shear zones are dextral. They are connected by a network of secondary shear zones (either dextral or sinistral). The few lineaments recognised in the low-strain domains correspond to a relatively well-developed foliation. By comparison with the shear zones, this foliation has an attitude consistent with an overall dextral shearing. Hence, the structure of the whole batholith is a large-scale analogue of the C/S structures seen in the field.

At the southernmost extremity of the batholith, the high-strain zones are wide and abundant and they show a more complex pattern than further north, whereas low-strain areas are sparse. In the transfer zone, the high-strain zones progressively become thinner and more localized. They are mainly confined in two NNE–SSW-trending groups, the main one on the eastern margin of the Closepet granite, and the other, less important, on its western margin. These two main high strain zones have also been recognised in the field as strongly deformed shear zones (Fig. 6), also described by Jayananda and Mahabaleswar (1991).

5.2. The gap

In the gap area, granitic sheets connecting both parts of the batholith display a general N160E (± 20°) trend, with a steep dip (the exact dip is unknown, because the outcrops are generally flat and do not allow their 3D-shape to be seen). They intrude a gneissic basement, whose foliation has the same attitude. As these sheets have been only recently recognised, no detailed structural study has been performed on them.

5.3. Northern intrusions

5.3.1. Field data

The northern intrusion zone is made of several granitic bodies with mutually intrusive relationships. These intrusions (Fig. 2) are elliptic in shape, with an approximately N135 long axis and an aspect ratio of about three. Detailed work has been focused on one of these intrusions, located near Hampi ruins, 10 km east of Hospet. The Hampi intrusion extends on both banks of the Tunghabadra river; it is elliptic, 50 km in length and 20 km in width. It shows clear, intrusive relationships with the surrounding rocks, which mainly consist of a previously emplaced pink, slightly porphyritic granite. The Hampi intrusion itself is made of an enclave- and phenocryst-free, medium-grained, grey granite. It appears isotropic in the field and no evidence

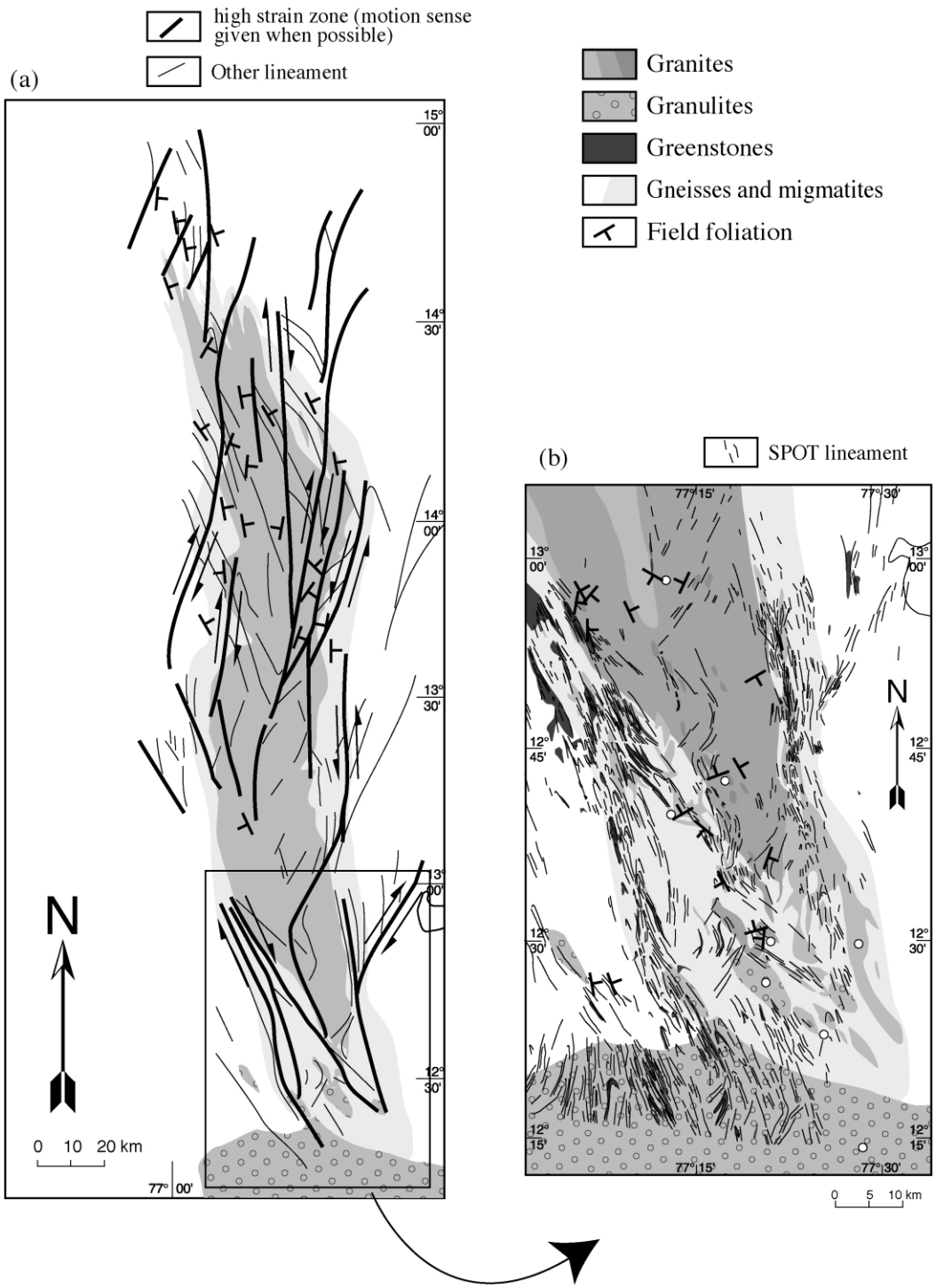

Fig. 10. Results of remote sensing photointerpretation. (a) Foliation trajectories and probable shear zones in the main mass of the Closepet granite. The Closepet granite is bounded on its eastern margin by an anastomosed network of shear zones, and in the West by a less-defined shear zone. In between, regular lineaments are interpreted as trace of foliation planes. (b) Detailed map of the root zone. High strain zones are apparent; they are wider, and do not define clear shear zones as in the North. Field-measured foliation planes are also indicated.

for solid-state deformation was found. These statements also apply to the pink enclosing granite.

5.3.2. Microstructures

All samples display magmatic microstructures with subhedral feldpars and interstitial quartz. Quartz crystals underwent incipient solid-state deformation at high-temperature conditions, as evidenced by prismatic and basal subgrains and a few recrystallised grains. Mylonitic microstructures were never observed.

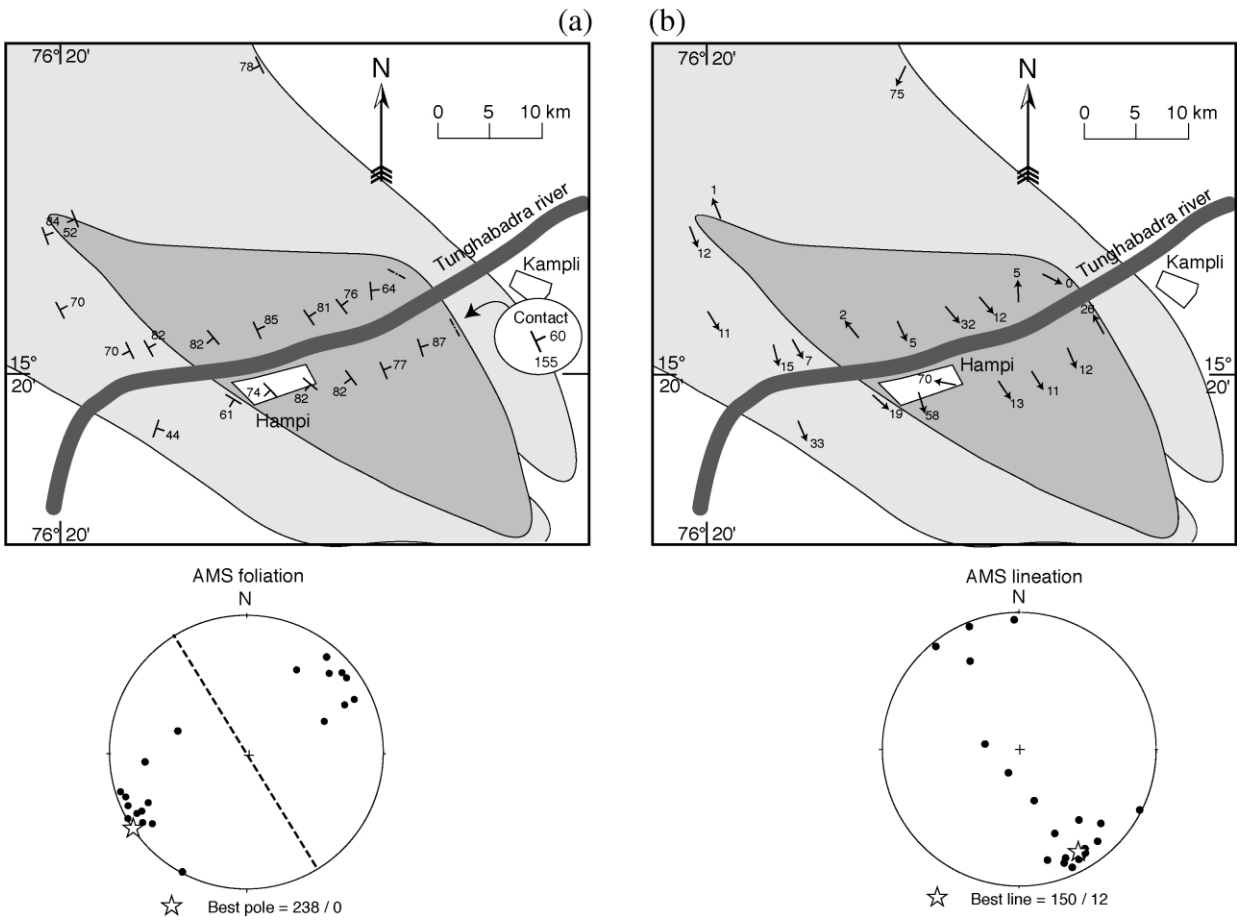

Fig. 11. AMS foliations (a) and lineations (b) in the Hampi intrusion. Tunghabadra river is represented by the SSW–NNE heavy line; Hampi intrusion is dark grey, whereas the surrounding, slightly porphyritic pink granite is in light grey.

The Hampi granite is a leucocratic rock, with scarce ferromagnesian and accessory minerals. Oxides (including magnetite) are euhedral grains, whose shape ratio ranges between 1 and 1.5. Shape preferred orientation of these slightly non-equant magnetite grains is therefore responsible for the magnetic fabrics.

5.3.3. AMS data

The magnetic fabric in the Hampi intrusion and surrounding granites is well-defined and displays a consistent pattern that can be seen in Table 2 and Fig. 11. The total magnetic anisotropy (P) ranges from 1.13 to 1.44, with an average value of 1.25. Although lower than in the main mass, these values are still higher than typical anisotropies for undeformed ferromagnetic plutonic rocks (Archanjo et al., 1992; Bouchez, 2000). Magnetic foliation planes (orthogonal to K_3) are well-defined, with an average strike northwest–southeast, parallel to the great axis of the Hampi intrusion, and a subvertical dip. The magnetic lineation is also well-defined, with an average orientation at 150/12 (Fig. 11b).

6. Discussion

6.1. Syntectonic emplacement of the Closepet batholith

Field and AMS data demonstrate that the Closepet granite was emplaced within an active strike-slip shear zone, as evidenced by steep foliation and subhorizontal lineation mostly parallel to the long axis of the batholith. The presence of both magmatic and solid-state deformation features demonstrates that this strike-slip event has been active during and after complete crystallisation of the magma. In the main mass, field observations of C/S obliquities as well as remote sensing data point to a dextral sense of motion. It is argued that the northern intrusions were also emplaced during the same shearing event, as deduced from their consistent magnetic fabrics and from their nearly coeval ages.

The close spatial and temporal relationships of granite plutons and shear zones may be interpreted either as a consequence of shear zone-assisted magma transfer and emplacement, or as the result of magma-enhanced strain localisation. Vauchez et al. (1997) discussed this point and attempted to review discriminating criteria in order to assess

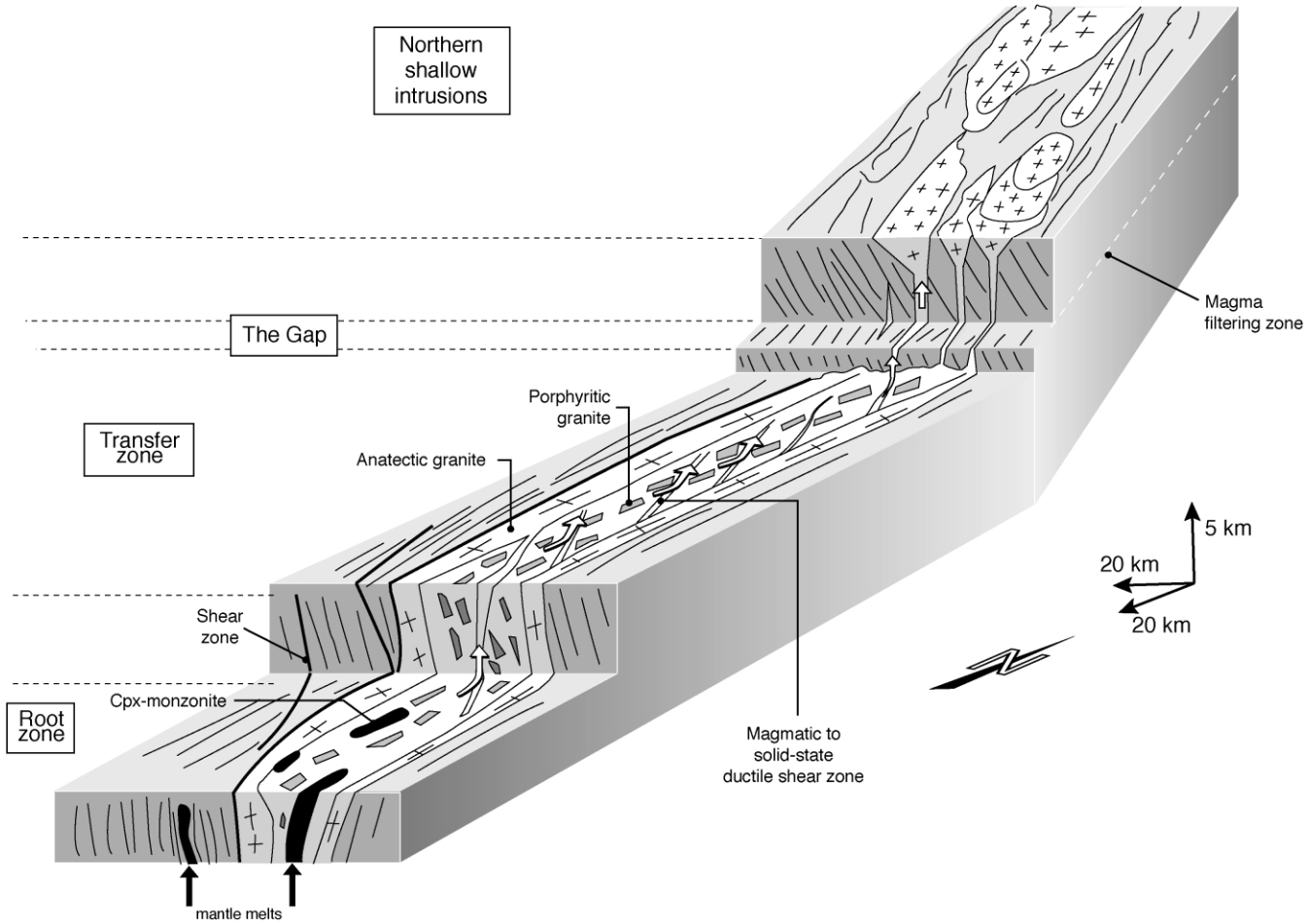

Fig. 12. 3D representation of the Closepet granite at different crustal levels; transfer of residual melt indicated by white arrows.

the respective anteriority of tectonism versus magmatism. Indeed, the Closepet main mass is an elongate intrusion, located in the vicinity of high-strain zones, and its magmatic to mylonitic structures are everywhere parallel to the solid-state deformation features recognised in the country rocks. For these reasons, emplacement of the Closepet main mass seems coeval with the transcurrent tectonics in the Dharwar craton.

However, this huge volume of magma likely influenced the mechanical behaviour of the crust. Magma emplacement along a subvertical shear zone allowed advective heat transfer through the crust, possibly responsible for a bulging of the isotherms in the vicinity of the shear zone, as documented for other crustal-scale, hundreds of kilometres long, shear zones (Leloup et al., 1995; Pili et al., 1997). Such a thermal anomaly may have enhanced the ductile deformation of the crust. It is therefore likely that tectonics and magmatism were involved in a positive feedback loop, as already proposed for Phanerozoic magmatic arcs in obliquely convergent settings (Saint Blanquat et al., 1998).

6.2. Magma ascent and emplacement at different structural levels

Data collected at different scales from different structural levels allow the following emplacement scenario for the Closepet granite to be proposed (Fig. 12).

6.2.1. Root zone

In the root zone, magma was partly intruded from deeper (mantle) levels, and partly produced by in-situ crustal melting (Jayananda et al., 1995; Moyen et al., 1997, 2001). Feeder zones might be identified by the presence of subvertical lineation, possibly more mafic facies, and pluton's floor deepening inferred from gravimetric data (Vigneresse and Bouchez, 1997). But steeply deeping lineations are hardly observed (Fig. 8b) in the root zone. Therefore, the so-called root zone does not display the typical features of a feeder zone. High strain areas (Fig. 10b), where magmatic sheets and dykes injected along ductile shear zones, are ubiquitous. This relatively dense network of high strain zones favoured and controlled magma collection. Besides, the low viscosity of the country rocks likely inhibited dyking and its consequent fast upward transfer of the magmas (Weinberg and Searle, 1998). Hence, the root zone became a mixing and mingling zone between the deeply-generated magmas and the anatectic melts derived from partial melting of the TTG-gneisses. Thereafter, the structures of the root zone have been

reoriented by magmatic flow and solid-state deformation after magma emplacement at this crustal level, thus obliterating witnesses of magma ascent.

6.2.2. Transfer zone

The transfer zone is characterised by the highest AMS anisotropies, as well as by a continuum from magmatic to orthogneissic structures, typical of syntectonic magmatism. Ubiquitous subhorizontal lineations together with steep foliations, that are also subparallel to the long axis of the batholith, as well as the very high shape ratio of the main mass of the Closepet granite, are strong evidence of magma emplacement during strike-slip shearing. Brown and Solar (1998) discussed a similar case and concluded that the transcurrent tectonic controls melt transfer in the crust, favouring lateral displacement rather than upward motion. In the case of the Closepet batholith, we consider this view to be oversimplified. Rather, we propose that liquid/solid partitioning occurred in the transfer zone, allowing the residual melt to escape upwards to feed the granitic sheets recognised in 'the Gap' and the shallow intrusions. Indeed, volume loss by residual melt expelling is suggested by the enclave-rich high-strain zones observed in the main mass.

From their study of the Alpine Bergell pluton, Rosenberg et al. (1995) contend that an intrusion emplaced in a transpressive regime can be squeezed at depth, thus expelling magma vertically to fill a ballooning upper emplacement site. Although a transpressive setting is not demonstrated for the Closepet Batholith, partitioning between the melt fraction and the solid fraction likely occurred similarly when the crystallising magma reached a critical crystalline load, the so-called rigid percolation threshold of Vigneresse et al. (1996). In felsic magmas, this threshold is estimated at around 55% solid fraction. At this stage, there is a weak framework of touching particles, where subvertical shear bands are able to nucleate during non-coaxial deformation. The residual melt can be expelled into these magmatic shear zones, that develop on a metre to kilometre scale. Thus, the magmatic foliation becomes more and more pronounced up to the particle locking threshold that is finally reached prior to full crystallisation (Vigneresse and Tikoff, 1999). This second threshold is estimated at around 75% solid fraction or more. Therefore, the large volume of melt (25–45%) present between the two thresholds is able to migrate both horizontally and vertically in the shear bands. It is worth noticing that the magmatic fabric of the transfer zone exclusively records the behaviour of the solid framework: there is no direct record of melt vertical flow. However, indirect evidence is provided by the vertical petrographic zoning of the Closepet batholith and by the high anisotropy recorded at the magmatic stage in the transfer zone. The last deformation stage occurred below the solidus, when increasing strain localisation led to C–S structures and mylonites (Gapais, 1989).

6.2.3. The Gap

The 'Gap' contains granitic sheets linking the Closepet main mass and the northern intrusions as represented in Fig. 10. The sheets are parallel to the foliation strike of the country-rocks, pointing to their emplacement during the same strike-slip tectonics, rather than dyke opening in tensile conditions. They formed as a consequence of overpressure of the residual liquids in the crystallizing main mass submitted to transpressive deformation. Thermobarometric data in the country rocks suggest that they were formed at around 500 °C and 4 kb, i.e. at depths within 12–15 km. These conditions cannot correspond to the steady-state ductile–brittle transition in a melt-devoid crust, where the rheology is likely controlled by quartz as the softer mineral phase (Handy, 1990), hence a ductile–brittle transition at about 350 °C (Kusznir and Park, 1986). Nevertheless, a transient brittle behaviour may result from the magmatic overpressure driven by magma squeezing at a deeper level (Williams et al., 1995). The gap is a peculiar level where magma filtering occurred and contributed to the vertical zonation of the whole magmatic complex.

6.2.4. Northern intrusions

With respect to the main mass, the northern intrusions have the more differentiated (only granitic) composition. They display a homogeneous and isotropic appearance in the field, lower magnetic anisotropy, lower shape ratios and no solid-state deformation. As already discussed, these petrographically evolved compositions are thought to result from a tectonically driven mechanism of solid–liquid partitioning, operating as filter-press, in the main mass. At the upper crustal level, due to a higher temperature contrast with country rocks, magma cools faster, thus diminishing the time available to develop a strong magmatic fabric. This effect is enhanced by the fact that granitic compositions crystallize along a narrower temperature interval than mafic or intermediate compositions (Bouchez et al., 1992). The exact opposite occurred at deeper levels, in the root and transfer zones, where intermediate magmas were emplaced at higher temperature and reached their solidus after a much longer time (Johannes and Holtz, 1996).

Nevertheless, the northern upper intrusions display magnetic fabrics that are in agreement with the syn-shearing emplacement recognised at depth. This magmatic fabric is characterised by a lower anisotropy than in the main mass, because it has been acquired during a shorter time interval within a narrow temperature range, due to the higher crustal level and faster cooling. After full crystallisation, solid-state plastic deformation did not take place inside the granites, which behaved as rigid bodies, but was restricted to narrow zones outside.

The combined width of the northern intrusions, larger than that of the main mass, is attributed to the fact that magmas can spread laterally at upper levels, which is difficult or impossible at lower levels (Romàn-Berdiel et al., 1997), since dilatant volumes are easier to create near to the

surface. However, their 3D shape remains a matter of speculation. By comparison with the gravity-modelled cases reviewed by Ameglio et al. (1997), we favour a wedge-shaped profile rather than a flat-floored one (Fig. 10) for these plutons emplaced during transcurrent tectonics.

7. Conclusions

The following conclusions can be drawn from this study:

1. The Closepet batholith was emplaced along a crustal-scale shear zone during a Late Archaean transcurrent event.
2. This shear zone probably acted as a channel for the intrusion of mantle-derived magmas and favoured their interaction with crustal-derived magmas. This trancurrent tectonic setting was also responsible for deformation-driven differentiation of the magmas in the lower to middle crust. Liquid–solid partitioning in the crystallising magmas enabled the residual liquids to rise upwards.
3. The Closepet batholith provides information on the mechanisms of transfer and emplacement of coeval magmas at different levels in the continental crust. Noticeably, steep foliations and subhorizontal lineations are similar throughout the batholith, characterising its syn-shearing emplacement.
4. The fabric intensity is controlled by the emplacement level and the compositions of the magmas. Development of strong magmatic to submagmatic fabric in the main mass results from the long residence times of intermediate to felsic magmas in the appropriate ranges of solid/liquid ratios during their crystallisation at depth. The shallower granitic northern intrusions did not experience such a long crystallisation history. Without the help of AMS data that unravelled and quantified their anisotropies, these northern intrusions would have appeared as post-tectonic, whereas the deeper main mass was obviously syn-tectonic, as evidenced by its strong magmatic and solid-state fabrics.
5. The gap, formed in P–T conditions around 500 °C and 4 kb, acts as a zone of magma filtering, leaving the solid components of the main mass at depth, and only allowing liquid ascent, hence the vertical zonation of the whole complex.

Acknowledgments

Field work was founded by IFCPAR (project 2307-1, “Accretionary processes of juvenile crust and continental growth: the late Archean Eastern Dharwar Craton”) and was possible only due to the help of Prof. Mahabaleswar, Bangalore university. P. Lespinasse was of greatest help during AMS measurement in Toulouse. AMS results have been treated using ‘EXAMS’, a program written by M. de Saint-Blanquat. P. Choukroune was the first to propose (in the field) the idea of syn-shearing emplacement for the Closepet granite; fruitful discussions with O. Merle, J.-L. Bouchez, P. Olivier and J.-J. Peucat greatly helped in the interpretation of data. Constructive reviews by A.M. Boullier and C. Rosenberg, as well as editorial assistance by T.G. Blenkinsop, are greatly acknowledged. Finally, we would like to dedicate this paper to the memory of B. Auvray, who was among the initiaters of the present work.

References

Ameglio, L., Vigneresse, J.L., Bouchez, J.L., 1997. Granite pluton geometry and emplacement mode inferred from combined fabric and gravity data. In: Bouchez, J.L., Hutton, D., Stephens, W.E. (Eds.), Granite: from Segregation of Melt to Emplacement Fabrics, Kluwer, Dordrecht, pp. 199–214.

Archanjo, C., Olivier, P., Bouchez, J.L., 1992. Plutons granitiques du Serido (NE du Brésil): écoulement magmatique parallèle à la chaîne révélé par leur anisotropie magnétique. Bulletin de la Société Géologique de France 163, 509–520.

Barker, F., Arth, J.G., 1976. Generation of trondhjemite–tonalite liquids and Archaean trondhjemite–basalt suites. Geology 4, 596–600.

Bateman, R., 1984. On the role of diapirism in the segregation, ascent and final emplacement of granitoids. Tectonophysics 10, 211–231.

Benn, K., Cruden, A.R., Sawyer, E.W. (Eds.), 1998. Extraction, transport and emplacement of granitic magmas. Journal of Structural Geology 20 (9/10).

Berthé, D., Choukroune, P., Jégouzo, P., 1979. Orthogneiss, mylonite and non-coaxial deformation of granites: the example of the South Armorican Shear Zone. Journal of Structural Geology 1, 31–42.

Borradaile, G., Henry, B., 1997. Tectonic applications of magnetic susceptibility and its anisotropy. Earth-Science Reviews 42, 49–93.

Bouchez, J.L., 1997. Granite is never isotropic: an introduction to AMS studies of granitic rocks. In: Bouchez, J.L., Hutton, D., Stephens, W.E. (Eds.), Granite: from Segregation of Melt to Emplacement Fabrics, Kluwer, Dordrecht, pp. 95–112.

Bouchez, J.L., 2000. Anisotropie de susceptibilité magnétique et fabrique des granites. Comptes-Rendus à l’Académie des Sciences de Paris 330, 1–14.

Bouchez, J.L., Tubia, J.M., Mainprice, D., 1985. Déformation naturelle du quartz: coexistence des systèmes de glissement de direction ⟨a⟩ et [c] à haute température (migmatites de la nappe d’Ojén, Espagne). Comptes-Rendus à l’Académie des Sciences de Paris 301, 841–846.

Bouchez, J.L., Delas, C., Gleizes, G., Nédélec, A., Cuney, M., 1992. Submagmatic microfractures in granites. Geology 20, 35–38.

Bouhallier, H., 1995. Evolution structurale et métamorphique de la croûte continentale archéenne (Craton de Dharwar, Inde du Sud). Mémoire de Géosciences Rennes n°60, Rennes, France.

Bouhallier, H., Chardon, D., Choukroune, P., 1995. Strain patterns in Archaean dome-and-basin structures: the Dharwar craton (Karnataka, South India). Earth and Planetary Science Letters 135, 57–75.

Brown, M., Solar, G.S., 1998. Shear-zone systems and melts: feedback relations and self-organization in orogenic belts. Journal of Structural Geology 20, 211–227.

Buhl, D., Grauert, B., Raith, M., 1983. U–Pb zircon dating of Archaean rocks from the south Indian craton: results from the amphibolite to

granulite transition zone at Kabbal quarry, Southern Karnataka. Fortschritte für Mineralogie 61, 43–45.

Chadwick, B., Vasudev, V.N., Ahmed, N., 1996. The Sandur schist belt and its adjacent plutonic rocks. Implications for late Archaean crustal evolution in Karnataka. Journal of the Geological Society of India 47, 37–57.

Chadwick, B., Vasudev, V.N., Hedge, G.V., 2000. The Dharwar Craton, Southern India, interpreted as the result of late Archean oblique convergence. Precambrian Research 99, 91–111.

Chardon, D., Choukroune, P., Jayananda, M., 1996. Strain patterns, decollement and incipient sagducted greenstone terrains in the Archaean Dharwar craton (south India). Journal of Structural Geology 18, 991–1004.

Chardon, D., Choukroune, P., Jayananda, M., 1998. Sinking of the Dharwar Basin (South India): implications for Archaean tectonics. Precambrian Research 91, 15–39.

Clemens, J.C., 1998. Observations on the origins and ascent mechanisms of granitic magmas. Journal of the Geological Society of London 155, 843–851.

Clemens, J.C., Mawer, C.K., 1992. Granitic magma transport by fracture propagation. Tectonophysics 204, 339–360.

Collins, W.J., Sawyer, E.W., 1996. Pervasive granitoid magma transfer through the lower-middle crust during non-coaxial compressional deformation. Journal of Metamorphic Geology 14, 565–579.

Crawford, A.R., 1969. Reconnaissance Rb–Sr dating of the Precambrian rocks of southern Peninsular India. Journal of the Geological Society of India 10, 117–166.

Déléris, J., Nédélec, A., Ferré, E., Gleizes, G., Ménot, R.P., Obasi, C.K., Bouchez, J.L., 1996. The Pan-African Toro Complex (northern Nigeria): magmatic interactions and structures in a bimodal intrusion. Geological Magazine 133, 535–552.

D'Lemos, R.S., Brown, M., Strachan, R.A., 1992. Granite magma generation, ascent and emplacement within a transpressional orogen. Journal of the Geological Society 149, 487–490.

Drury, S.A., Harris, N.B., Holt, R.W., Reeves-Smith, G.J., Wightman, R.T., 1984. Precambrian tectonics and crustal evolution in South India. Journal of Geology 92, 3–20.

Ellwood, B.B., Whitney, J.A., 1980. Magnetic fabric of the Elberton granite, northeast Georgia. Journal of Geophysical Research 85, 1481–1486.

Friend, C.R.L., 1984. The origin of the Closepet granites and the implications for the crustal evolution of Southern India. Journal of the Geological Society of India 25, 73–84.

Friend, C.R.L., Nutman, A.P., 1991. Shrimp U–Pb geochronology of the Closepet granite and Peninsular gneiss, Karnataka, South India. Journal of Geological Society of India 38, 357–368.

Gapais, D., 1989. Shear structures within deformed granites: mechanical and thermal indicators. Geology 17, 1144–1147.

Gopalakrishna, D., Hansen, E.C., Janardhan, A.S., Newton, R.C., 1986. The Southern high-grade margin of the Dharwar craton. Journal of Geology 94, 247–260.

Graham, J.W., 1954. Magnetic susceptibility anisotropy: an unexploited petrofabric element. Geological Society of America, Abstracts with Programs 65, 1257–1258.

Grégoire, V., Darrozes, J., Gaillot, P., Nédélec, A., Launeau, P., 1998. Magnetite grain shape fabric and distribution anisotropy vs rock magnetic fabric: a three-dimensional case study. Journal of Structural Geology 20, 937–944.

Grew, E.S., Manton, W.I., 1984. Age of allanite from Kabbaldurga quarry, Karnataka. Journal of the Geological Society of India 25, 193–195.

Handy, M., 1990. The solid state flow of polymineralic rocks. Journal of Geophysical Research 95, 8647–8661.

Hansen, E.C., Newton, R.C., Janardhan, A.S., 1984. Pressures, temperatures and metamorphic fluids across an ubroken amphibolite facies to granulite facies transition in Southern Karnataka. In: Kröner, A., (Ed.), Archaean Geochemistry, Springer Verlag, Berlin, pp. 161–181.

Harris, N.B.W., Jayaram, S., 1982. Metamorphism of cordierite gneisses from the Bangalore region of the Indian Archaean. Lithos 15, 89–98.

Hutton, D.H.W., Reavy, R.J., 1992. Strike-slip tectonics and granite petrogenesis. Tectonics 11, 960–967.

Hutton, D.H.W., Dempster, T.J., Brown, P.E., Becker, S.D., 1990. A new mechanism of granite emplacement: intrusion in active extensional shear zones. Nature 343, 452–455.

Ishihara, S., 1977. The magnetite-series and ilmenite-series granitic rocks. Mining Geology (Tokyo) 27, 293–305.

Janardhan, A.S., Newton, R.C., Hansen, E.C., 1982. The transformation of amphibolite facies gneiss to charnockite in Southern Karnataka and Northern Tamil Nadu, India. Contributions to Mineralogy and Petrology 119, 130–149.

Jayananda, M., Mahabaleswar, B., 1991. Relationships between shear zones and igneous activity: the Closepet granite of Southern India. Proceedings of the Indian Academy of Sciences 100, 31–36.

Jayananda, M., Martin, H., Peucat, J.-J., Mahabaleswar, B., 1995. Late Archaean crust-mantle interactions: geochemistry of LREE-enriched mantle derived magmas. Example of the Closepet batholith, southern India. Contributions to Mineralogy and Petrology 119, 314–329.

Jayananda, M., Moyen, J.F., Martin, H., Peucat, J.-J., Auvray, B., Mahabaleswar, B., 2000. Late Archaean (2550–2520 Ma) juvenile magmatism in the Eastern Dharwar craton, southern India: constraints from geochronology, Nd–Sr isotopes and whole rock geochemistry. Precambrian Research 99, 225–254.

Jelinek, V., 1981. Characterization of the magnetic fabrics of rocks. Tectonophysics 79, 63–67.

Johannes, W., Holtz, F., 1996. Petrogenesis and Experimental Petrology of Granitic Rocks, Springer-Verlag, Berlin.

Krogstad, E.J., Hanson, G.N., Rajamani, V., 1991. U–Pb ages of zircon and sphene for two gneiss terranes adjacent to the Kolar schist belt, South India: evidence for separate crustal evolution histories. Journal of Geology 99, 801–816.

Kruhl, J.H., 1996. Prism- and basal-plane parallel subgrain boundaries in quartz: a microstructural geothermobarometer. Journal of Metamorphic Geology 14, 581–589.

Kusznir, N.J., Park, R.G., 1986. Continental lithosphere strength: the critical role of lower crustal deformation. In: Dawson, J.B., Carswell, D.A., Hall, J., Wedepohl, K.H. (Eds.), The Nature of the Lower Continental Crust. Geological Society Special Publication 24, pp. 79–93.

Launeau, P., Cruden, A., 1998. Magmatic fabric acquisition mechanisms in a syenite: results of a combined anisotropy of magnetic susceptibility and image analysis study. Journal of Geophysical Research 103, 5067–5089.

Leloup, P.H., Lacassin, R., Tapponier, P., Schärer, U., Zhong, D., Liu, X., Zhang, L., Ji, S., Phan, T.T., 1995. The Ailao Shan–Red River shear zone (Yunnan, China), Tertiary transform boundary of Indochina. Tectonophysics 251, 3–84.

Mahabaleswar, B., Jayananda, M., Peucat, J.-J., Shadakshara Swamy, N., 1995. Archaean high-grade gneiss complex from Satnur–Halagur–Sivasamudram area, Karanataka, Southern India: petrogenesis and crustal evolution. Journal of the Geological Society of India 45, 33–49.

Martelat, J.-E., Vidal, G., Lardeaux, J.-M., Nicollet, C., Rakotondrazafy, R., 1995. Images spatiales et tectonique profonde des continents: l'exemple du Sud-Ouest de Madagascar. Comptes-rendus à l'Académie des Sciences de Paris 321, 325–332.

Martin, H., 1994. The Archaean grey gneisses and genesis of continental crust. In: Condie, K.C. (Ed.), Archaean Crustal Evolution. Developments in Precambrian Geology 11, Elsevier, pp. 205–259.

Meen, J.K., Rogers, J.J.W., Fullargar, P.D., 1992. Lead isotopic compositions of the Western Dharwar Craton, southern India: evidence for distinct middle Archean terranes in a late Archean craton. Geochimica et Cosmochimica Acta 56, 2455–2470.

Moyen, J.-F., 2000. Le magmatisme granitique à la transition Archéen-Protérozoïque: exemple du craton de Dharwar, Inde du Sud (Granite de Closepet et intrusions associées). PhD. thesis, Université Blaise Pascal, Clermont-Ferrand, France.

Moyen, J.-F., Martin, H., Jayananda, M., 1997. Origine du granite finiarchéen de Closepet (Inde du Sud): apports de la modélisation

géochimique du comportement des éléments en trace. Comptes-rendus à l'Académie des Sciences de Paris 325, 659–664.

Moyen, J.-F., Martin, H., Jayananda, M., 2001. The Closepet granite (S. India) multi-elements geochemical modelling of Crust–Mantle interactions during late-Archaean crustal growth. Precambrian Research 112, 87–105.

Nédélec, A., Ralison, B., Bouchez, J.L., Grégoire, V., 2000. Structure and metamorphism of the granitic basement around Antananarivo: a key to the Pan-African history of central Madagascar and its Gondwana connections. Tectonics 19, 997–1020.

Newton, R.C., 1990. Fluids and melting in the Archaean deep crust of southern India. In: Ashworth, J.C., Brown, M. (Eds.), High-temperature Metamorphism and Crustal Anatexis, Unwin Hyman, pp. 149–179.

Nutman, A.P., Chadwick, B., Krishna Rao, B., Vasudev, V.N., 1996. SHRIMP U–Pb zircon ages of acid volcanic rocks in the Chitradurga and Sandur Groups and granites adjacent to Sandur schist belt. Journal of the Geological Society of India 47, 153–161.

Paterson, S.R., Fowler, K.F. Jr, 1993. Re-examining pluton emplacement processes. Journal of Structural Geology 15, 191–206.

Paterson, S.R., Miller, R.B., 1990. Mid-crustal magmatic sheets in the cascades Mountains, Washington: implications for magma ascent. Journal of Structural Geology 20, 1345–1363.

Petford, N., 1996. Dykes or diapirs? Transactions of the Royal Society of Edinburgh 87, 105–114.

Peucat, J.-J., Bernard-Griffiths, J., Condie, K.C. Sr, 1989. Nd and Pb isotopic systematics in the Archaean low- to high-grade transition zone of Southern India: syn-accretion vs. post-accretion granulites. Journal of Geology 97, 537–550.

Peucat, J.-J., Mahabaleswar, M., Jayananda, M., 1993. Age of younger tonalitic magmatism and granulite metamorphism in the amphibolite–granulite transition zone of southern India (Krishnagiri area): comparison with older Peninsular gneisses of Gorur–Hassan area. Journal of Metamorphic Geology 11, 879–888.

Peucat, J.-J., Bouhallier, H., Fanning, C.M., Jayananda, M., 1995. Age of Holenarsipur schist belt, relationships with the surrounding gneisses (Karnataka, south India). Journal of Geology 103, 701–710.

Pichamuthu, C.S., 1961. Transformation of Peninsular gneiss into charnockite in Mysore State, India. Journal of Geological Society of India 2, 46–49.

Pili, E., Ricard, Y., Lardeaux, J.M., Sheppard, S.M.F., 1997. Lithospheric shear zones and mantle–crust connections. Tectonophysics 280, 15–29.

Raase, P., Raith, M., Ackermand, D., Lal, R.K., 1986. Progressive metamorphism of mafic rocks from greenschist to granulite facies in the Dharwar craton of South India. Journal of Geology 94, 261–282.

Rochette, P., 1987. Magnetic susceptibility of the rock matrix related to magnetic fabric studies. Journal of Structural Geology 9, 1015–1020.

Rochette, P., Jackson, M., Aubourg, C., 1992. Rock magnetism and the interpretation of anisotropy of magnetic susceptibility. Review of Geophysics 30, 209–226.

Rollinson, H.R., Windley, B.F., Ramakrishnan, M., 1981. Contrasting high and intermediate pressures of metamorphism in the Archaean Sargur schists of southern India. Contributions to Mineralogy and Petrology 76, 420–429.

Romàn-Berdiel, T., Gapais, D., Brun, J.P., 1997. Granite intrusion along strike-slip zones in experiment and nature. American Journal of Science 297, 651–678.

Rosenberg, C.L., Berger, A., Schmid, S.M., 1995. Observations from the floor of a granitoid pluton: inferences on the driving force of final emplacement. Geology 23, 443–446.

Saint Blanquat, M. de, Tikoff, B., 1997. Development of magmatic to solid-state fabrics during syntectonic emplacement of the Mono Creek granite, Sierra Nevada batholith. In: Bouchez, J.L., Hutton, D., Stephens, W.E. (Eds.), Granite: from Segregation of Melt to Emplacement Fabrics, Kluwer, Dordrecht, pp. 231–252.

Saint Blanquat, M. de, Tikoff, B., Teyssier, C., Vigneresse, J.L., 1998. Transpressional kinematics and magmatic arcs. In: Holdsworth, R.E., Strachan, R.A., Dewey, J.F. (Eds.), Continental Transpressional and Transtensional Tectonics, Geological Society Special Publication, London, 135, pp. 327–340.

Sen, S.K., Bhattacharya, K., 1990. Granulites of Satnuru and Madras area: a study in different behaviors of fluids. In: Vielzeuf, D., Vidal, P. (Eds.), Granulites and Crustal Evolution, NATO ASI series, serie C, vol. 311, pp. 367–384.

Srinivasan, R., Tareen, J.A.K., 1972. Andalusite from the Hospet area, Sandur Schist Belt, Mysore state. Indian Mineralogist 13, 42–45.

Stähle, H.J., Raith, M., Hoernes, S., Delfs, A., 1987. Element mobility during incipient granulites formation at Kabbaldurga, Southern India. Journal of Petrology 28, 803–834.

Taylor, P.N., Chadwick, B., Moorbath, S., Ramakrishanan, M., Viswanatha, M.N., 1984. Petrography, chemistry and isotopic ages of Peninsular Gneisses, Dharwar acid volcanics and Chitradurga granites with special reference to Archaean evolution of Karnataka craton, southern India. Precambrian Research 23, 349–375.

Vauchez, A., Neves, S.P., Tommasi, A., 1997. Transcurrent shear zones and magma emplacement in Neoproterozoic belts of Brazil. In: Bouchez, J.L., Hutton, D., Stephens, W.E. (Eds.), Granite: from Segregation of Melt to Emplacement Fabrics, Kluwer, Dordrecht, pp. 275–293.

Vigneresse, J.L., Bouchez, J.L., 1997. Successive granitic magma batches during pluton emplacement: the case of Cabeza de Araya (Spain). Journal of Petrology 38, 1767–1776.

Vigneresse, J.L., Tikoff, B., 1999. Strain partitioning during partial melting and crystallizing felsic magmas. Tectonophysics 312, 117–132.

Vigneresse, J.L., Barbey, P., Cuney, M., 1996. Rheological transitions during partial melting and crystallization with application to felsic magma segregation and transfer. Journal of Petrology 37, 1579–1600.

Weinberg, R.F., Searle, M.P., 1998. The Pangong Injection Complex, Indian Karakoram: a case of pervasive granite flow through hot viscous crust. Journal of the Geological Society 155, 883–891.

Williams, M.L., Hanmer, S., Kopf, C., Darrach, M., 1995. Syntectonic generation and segregation of tonalitic melts from amphibolite dikes in the lower crust, Striding–Athabasca mylonite zone, northern Saskatchewan. Journal of Geophysical Research 100, 15717–15734.

Windley, B.F., 1995. The Evolving Continents, 3rd edition, Wiley, Chichester.